3D hygro-elastic shell model for the analysis of composite and sandwich structures

3D hygro-elastic shell model for the analysis of composite and sandwich structures

S. Brischetto* and R. Torre

Department of Mechanical and Aerospace Engineering, Politecnico di Torino, Torino, Italy

Abstract *The present work proposes the study of the hygrometric loading effects in the static analysis of multilayered composite and sandwich plates and shells. The employed model is based on a general exact 3D shell theory valid for one-layered and multilayered sandwich and composite plates, cylinders and cylindrical/spherical shell panels. The employed 3D equilibrium equations are developed in an orthogonal mixed curvilinear coordinate system for spherical shells in order to obtain the other simpler geometries as particular cases. A layer-wise approach is employed and equilibrium equations are solved in the thickness direction via the exponential matrix method. The partial derivatives in the in-plane directions are exactly calculated by assuming simply-supported edges and harmonic forms for the variables. The presented 3D shell model is extended to hygro-elastic cases by considering moisture content amplitudes imposed at the external surfaces of the structures in steady-state conditions. The moisture content profile through the thickness of the structures can be included in the 3D shell model using three different methodologies: it can be calculated by solving the steady-state 3D or 1D version of the Fick diffusion law, or it can be "a priori" assumed as linear through the thickness. Therefore, the developed system includes three non-homogeneous second order differential equilibrium equations that are solved after the introduction of opportune mathematical layers to consider the curvature effects through the thickness. The reduction to a first order differential equation system is obtained by redoubling the number of variables. The exponential matrix method is employed to accurately define both general and particular solutions. The implemented 3D hygro-elastic shell model is firstly validated and then it is employed with confidence for new benchmarks where the effects of thickness ratio, geometry, lamination scheme, material, thickness layer and imposed moisture content values at the external surfaces are investigated for composite and sandwich plates and shells. Showed results demonstrate the importance of an accurate developing of the elastic part of the 3D shell model combined with an appropriate evaluation of the moisture content profile through the thickness. Assumed linear moisture content profiles are correct only for thin one-layered isotropic structures, the use of the 1D Fick diffusion law allows only the correct definition of the material layer effect, the use of its 3D version allows the correct definition of both material and thickness layer effects.*

Keywords: 3D exact hygro-elastic shell model; linear moisture content profile; 3D and 1D versions of Fick diffusion law; sandwich and composite plates and shells; hygro-elastic stresses.

*Author for Correspondence: Salvatore Brischetto, Department of Mechanical and Aerospace Engineering, Politecnico di Torino, corso Duca degli Abruzzi 24, 10129 Torino, ITALY. tel: +39.011.090.6813, fax: +39.011.090.6899, e.mail: salvatore.brischetto@polito.it.

1 Introduction

Modern composite aircraft are often subjected to adverse environmental conditions with high temperatures and significant humidity levels. Aviation materials, and in particular composites, tend to absorb moisture and therefore they degrade the structural performance [1]. Composite materials degrade their mechanical properties when aircraft fly in typical operating environments because the moisture is absorbed from humid air. This effect is more remarked for the matrix material than the fibres [2]. The hygrothermal effects can be analyzed as degradation of mechanical properties of the embedded materials and/or as hygroscopic and thermal load applications on structures to evaluate their typical bending behavior [3], [4].

The proposed 3D shell model considers the hygro-elastic bending behavior of multilayered composite structures and it discards the property degradations. Strains linked with the moisture expansion of a multilayered structure have a magnitude similar to strains linked with the thermal expansion. The Fickian diffusion problem in composite structures allows the calculation of temperature and moisture content in composite structures when the following conditions are followed [5]: the heat transfer through the material is a conduction problem governed by the Fourier heat conduction law; the moisture diffusion through the material is governed by the Fick diffusion law; the temperature in the material arrives to the equilibrium much faster than the moisture concentration, this feature allows to decouple energy (Fourier) and mass transfer (Fick) equations; the thermal conductivity and mass diffusivity depend only on the temperature and not on the moisture concentration for typical stress levels in the material. Fickian diffusion is valid for low temperatures when materials are exposed to humid air. Deviations from Fickian diffusion are possible at high temperatures and/or for materials included in liquids. This described Fickian diffusion is a good approximation for many materials, also including graphite-epoxy composites [5], [6]. The proposed 3D shell model is an analytical solution where the 3D equilibrium equations are written in orthogonal mixed curvilinear coordinates valid for spherical shells, cylindrical shells and plates. The derivatives with respect to the in-plane coordinates α and β are exactly solved by means of the harmonic forms while the system of differential equations in z is solved via the exponential matrix method. The first author applied this methodology the first time in 2013 and 2014 for the free vibration analysis of functionally graded [7], composite and sandwich [8] plates and shells. Then, the model was extended to the static analysis of multilayered composite structures in [9]. The exponential matrix method was successfully applied in the past to the free vibration analysis of multilayered plates in [10] and to the free vibration analysis of cylinders in [11]. A similar methodology was also used by Fan and Zhang [12] where the 3D equilibrium equations were written in orthogonal mixed curvilinear coordinates for spherical shells by assuming as primary variables the three displacement components and the three transverse stress components; in the present model, the main six primary variables are the three displacement components and their three derivatives in z. Fan and Zhang [12] used the Cayley-Hamilton theorem, while the present procedure employs the exponential matrix method combined with a large number of mathematical layers in order to correctly analyze also very thick shells giving a correct 3D description of displacements and stresses through the thickness. The static version of the 3D shell model developed in [9] for the bending analysis of structures was extended to the thermo-elastic analysis of spherical and cylindrical multilayered composite and sandwich shells and plates in [13] and for functionally graded material configurations in [14]. In 2018, the first author, in collaboration with Tornabene, developed the solution of the 3D equilibrium equations written in orthogonal mixed curvilinear coordinates using the Generalized Differential Quadrature Method (GDQM) to numerically solve the partial derivatives in z in order to perform the static analysis of multilayered composite and sandwich plates and completely double-curved shells when subjected to several combinations of transverse shear and transverse normal loads applied at the external surfaces [15], [16]. Recently, in 2020, this methodology was taken up by Monge and his co-authors [17]- [19] to perform numerical 3D elastic and thermo-elastic analyses of plates and spherical shells. The exact 3D shell model developed in

[7]- [9] by means of the exponential matrix method is here extended for the first time to the hygroelastic analysis of plates and shells using the analogy with the 3D methodologies already described in [13] and [14] for the thermo-elastic analysis of multilayered composite and functionally graded material structures. This analogy was already suggested by the first author in his past works about the developing of refined 2D thermo-hygro-elastic shell models [20], [21].

Several 2D analytical and numerical models are present in the literature for the hygroscopic stress analysis of multi-layered plates and shells. To the best of authors' knowledges, no exact 3D general shell models for plates and shells with constant radii of curvature have been yet developed for the hygroscopic stress analysis of multi-layered structures with the possibility of including several mathematical models for the evaluation of moisture content profiles through the thickness direction.

An analytical 2D solution for multi-layered plates was developed by Chiba and Sugano [22] for the hygrothermal stress analysis when structures were subjected to hygrothermal loads at the external surfaces; both steady-state and transient-state conditions were investigated and opportunely compared. In [23] and [24], analytical Classical Lamination Plate Theory (CLPT) was compared with analytical 3D plate models in the case of hygrothermoelastic analysis of multi-layered structures. The Fick diffusion equation was solved for transient and cyclical environmental conditions in order to find the moisture content profile. Mechanical and hygrothermal loadings were applied to plates with a central hole in [25], stresses were analysed via analytical and Finite Elements (FE) models. An analytical study for the hygrothermal stress analysis in laminated composite plates was proposed in [26] where Classical Lamination Theory (CLT) and Tsai-Wu failure criterion were applied. A composite cylindrical panel was analytically investigated in [27] via a 3D analysis when hygrothermal and mechanical loads were applied. Hygrothermal buckling and post-buckling analytical studies of multi-layered composite cylindrical shells were performed by Shen [28] using the Reddy higher order theory. In the analytical model by Sih [29] for stress analysis of composites, the moisture diffusion coefficient was a function of the temperature while the thermal diffusion coefficient was constant. Wüthrich [30] proposed the hygrothermal stress analysis for long multi-layered composite tubes when internal and external pressures were applied. Zenkour [31] extended these types of problems to functionally graded material (FGM) plates where elastic coefficients, thermal coefficients and moisture expansion coefficients continuously change through the thickness direction: an analytical Higher order Shear Deformation Theory was developed. Lee et al. [32] demonstrated how the classical laminated plate theory could be not adequate for the hygrothermal analysis of multilayered composite plates even if small deflections were considered. Upadhyay et al. [33] developed an Higher order Shear Deformation Theory (HSDT) combined with Von Karman non linear model for the non-linear flexural response of thick composite plates when hygro-thermo-mechanical loads were applied, HSDT showed some problems in such analyses. Limitations of classical lamination plate theory were deeply discussed in [34] for the application of mechanical, thermal and hygroscopic loads to composite structures. Boukert et al. [35] proposed an analytical method to investigate the behaviour of thick composite laminates using a high order plate theory via hygrothermal stress calculation; the moisture distribution was calculated along the thickness of the laminate using the Fick equation.

The above analytical methods can be applied only for particular geometries, load and boundary conditions and lamination schemes. For engineering applications, the use of numerical models (e.g., the Finite Element method (FEM)) is mandatory in order to overcome the main limitations of the analytical methods. A Finite Element plate model was developed in [36] to investigate the moisture content effects and the delamination problems in viscoelastic sandwich composite structures when subjected to mechanical loads. The finite element model by Khoshbakht et al. [37] analysed the hygrometric stresses in multilayered structures; the stresses at the interfaces increased when the moisture content diffusion increased in time, these stresses reached the steady state hygroscopic stress level. Kundu and Han [38] developed a Finite Element model to investigate the hygro-thermo-elastic vibration and buckling behaviour of multilayered composite doubly curved shell panels. The same authors investigated

hygrothermal stress effects on the buckling and dynamic instability of composite shell structures in [39] where a geometrically nonlinear finite element method was developed using the orthogonal curvilinear coordinate for general doubly curved deep or shallow shell structures. Marques and Creus [40] developed a FE shell model that used the Fick diffusion law for the hygrothermoelastic analysis of isotropic and multi-layered composite structures. The FE higher order shear deformation model by Naidu and Sinha [41] allowed the investigation of bending large deflections of composite cylindrical shell panels in hygrothermal environment. Parhi et al. [42] developed a quadratic isoparametric FE model employing the first order shear deformation theory for the free vibration and transient response analysis of multi-layered composite plates and shells subjected to hygrothermal effects. Hygrothermal static and dynamic analyses of laminated structures were proposed in [43] by using an higher-order Finite Element model. Sai Ram and Sinha [44], [45] evaluated the moisture content and temperature effects in the bending analysis of multi-layered composite plates in both cases of inclusion and discarding of a cutout; a Finite Element Mindlin plate model was used for these stress investigations. Sereir et al. [46]- [48] proposed the transient hygroscopic stress analysis in multi-layered composite plates when the elastic properties change with the temperature and moisture content variations. The solution in time of the diffusion Fick equations was possible via a Finite Element model that also included the edge effects. The Finite Element model in [49] allowed the study of initiation and progress of damage in multi-layered composite shells subjected to high moisture concentration and temperature fields when low velocity impacts were applied. A coupled piezoelectric finite element formulation including hygrothermal strains was developed in [50] to evaluate the active stiffness effects on the dynamic behaviour of piezo-hygro-thermo-elastic laminates. The work [51] proposed an approximate model to evaluate hygrothermoelastic stresses in composite laminated plates when the moisture desorption modified mechanical characteristics induced by the variation of temperature and moisture.

Further papers only considered the degradation of material properties in severe hygroscopic conditions. Chateauminois et al. [52] proposed three-point bending tests to study the fatigue phenomenology in composites linked with the effects of water ageing. Kellas et al. [53] proposed experimental results to show hygrothermal effects in uniaxial strengths of centre-notched laminates. These effects depended on the notch geometry and stacking sequence. Analytical stress and strain models were compared with experimental results in [54] to show how the elastic properties of glass/epoxy woven-fabric composites changed with the hygrothermal load variations. Springer [55] evaluated the moisture content distribution in composite materials exposed to air with variable temperature and relative humidity. The hygroscopic analysis of woven fabric carbon-epoxy composites was proposed in [56] where effects on the viscoelastic properties and glass transition temperature were also analyzed.

The present paper is organized in the following way. Section 2 proposes the solution of the 3D exact hygro-elastic shell model using the exponential matrix method. Section 3 discusses the moisture diffusion problem and its solution in analogy with the heat conduction problem. The analogy between heat conduction and moisture diffusion problems was also demonstrated in [57] where very useful hygrothermal bending problems of multi-layered composite structures were proposed. Such an analogy was also discussed in Tay and Goh [58], [59] where a complete numerical study was proposed. The Fick second law of diffusion was experimentally analyzed in Di Domizio et al. [60] by employing two vessels containing water and salt in order to establish a steady-state concentration gradient. In section 3, for both plate and shell geometries, the 3D version of Fick diffusion law is solved with the same methodology proposed in Tungikar and Rao [61] in the case of the solution of the Fourier heat conduction equations. In this section, the 1D version of the Fick diffusion law and the a priori linear assumption for the moisture content profile are also discussed in depth. Section 4 is about results, the first part proposes a validation of the model using the well-known 3D elastic solutions by Pagano [62] and Ren [63] and opportune 3D hygro-elastic FE models developed in the framework of the Patran & Nastran software. The second part shows new benchmarks to discuss the effects of geometry, material, lamination scheme, thickness ratio and moisture content profiles. Finally, section 5 is devoted to the main conclusions and

further developments.

2 3D exact hygro-elastic shell model

In order to develop the 3D exact hygro-elastic shell model, the main ingredients are the appropriate constitutive and geometrical equations, that must be opportunely substituted in the 3D equilibrium equations for shells written using the orthogonal mixed curvilinear coordinates (α, β, z) indicated in Figure 1. The final system contains three differential equations of second order in z with non-constant coefficients. The introduction of opportune mathematical layers and the redoubling of the number of variables give a system of three differential equations of first order in z with constant coefficients. The partial derivatives in in-plane directions α and β were exactly solved using simply-supported boundary conditions and harmonic forms for variables. The final system contains three differential equations with constant coefficients and first order partial derivatives in z. This system is non-homogeneous because of the known terms given by the presence of the moisture content profile. Both general and particular solutions are obtained by employing the exponential matrix method.

The multilayered shell is subjected to a moisture content $\mathcal{M}(\alpha, \beta, z)$. For each k physical layer, the geometrical relations written in an orthogonal mixed curvilinear reference system (α,β,z) are:

$$\epsilon^k_{\alpha\alpha} = \epsilon^k_{\alpha\alpha m} - \epsilon^k_{\alpha\alpha\mathcal{M}} = \frac{1}{H_\alpha}\frac{\partial u^k}{\partial \alpha} + \frac{w^k}{H_\alpha R_\alpha} - \eta^k_\alpha \mathcal{M}^k \ , \tag{1}$$

$$\epsilon^k_{\beta\beta} = \epsilon^k_{\beta\beta m} - \epsilon^k_{\beta\beta\mathcal{M}} = \frac{1}{H_\beta}\frac{\partial v^k}{\partial \beta} + \frac{w^k}{H_\beta R_\beta} - \eta^k_\beta \mathcal{M}^k \ , \tag{2}$$

$$\epsilon^k_{zz} = \epsilon^k_{zzm} - \epsilon^k_{zz\mathcal{M}} = \frac{\partial w^k}{\partial z} - \eta^k_z \mathcal{M}^k \ , \tag{3}$$

$$\gamma^k_{\beta z} = \gamma^k_{\beta z m} = \frac{1}{H_\beta}\frac{\partial w^k}{\partial \beta} + \frac{\partial v^k}{\partial z} - \frac{v^k}{H_\beta R_\beta} \ , \tag{4}$$

$$\gamma^k_{\alpha z} = \gamma^k_{\alpha z m} = \frac{1}{H_\alpha}\frac{\partial w^k}{\partial \alpha} + \frac{\partial u^k}{\partial z} - \frac{u^k}{H_\alpha R_\alpha} \ , \tag{5}$$

$$\gamma^k_{\alpha\beta} = \gamma^k_{\alpha\beta m} = \frac{1}{H_\alpha}\frac{\partial v^k}{\partial \alpha} + \frac{1}{H_\beta}\frac{\partial u^k}{\partial \beta} \ , \tag{6}$$

($\epsilon^k_{\alpha\alpha}$, $\epsilon^k_{\beta\beta}$, ϵ^k_{zz}, $\gamma^k_{\beta z}$, $\gamma^k_{\alpha z}$, $\gamma^k_{\alpha\beta}$) are the six strain components in each k physical layer. Each component is the algebraic summation of mechanical elastic strain components (subscript m) and hygroscopic strain components (subscript $\mathcal{M}$). The hygro-elastic strains are linked with the three displacement components u^k, v^k and w^k defined in α, β, z directions, respectively, and with the scalar moisture content $\mathcal{M}^k$. Moisture expansion coefficients η^k_α, η^k_β and η^k_z are given in the structural reference system (α, β, z) after the appropriate rotations of the moisture expansion coefficients η^k_1, η^k_2 and η^k_3 defined in the material reference system (1, 2, 3). The symbol ∂ indicates the partial derivatives.

The parametric coefficients H_α and H_β are functions of z (referred in the Ω_0 middle surface of the whole multilayer and variable from -h/2 to +h/2 where h is the global thickness) or $\tilde{z}$ (variable from 0 to h and referred to the bottom surface). Coefficients H_α and H_β are linear functions of the thickness coordinate z for shells with constant radii of curvature R_α and R_β in α and β directions, respectively. $H_z = 1$ because the z or $\tilde{z}$ coordinate is rectilinear:

$$H_\alpha = \left(1 + \frac{z}{R_\alpha}\right) = \left(1 + \frac{\tilde{z} - h/2}{R_\alpha}\right) , \tag{7}$$

$$H_\beta = \left(1 + \frac{z}{R_\beta}\right) = \left(1 + \frac{\tilde{z} - h/2}{R_\beta}\right) . \tag{8}$$

The scalar moisture content $\mathcal{M}$ can be defined in non-dimensional form or in percentage % (by multiplying it for 100):

$$\mathcal{M}(\%) = \frac{W - W_d}{W_d} \times (100) = \frac{W_d + W_c - W_d}{W_d} \times (100) = \frac{W_c}{W_d} \times (100)\,, \tag{9}$$

the global mass of the moist material is defined as $W = W_d + W_c$ where W_c is the mass of the included moisture and W_d is the mass of the dry material. The mass of the moisture included in the material can be defined by means of the integration in the volume V of the moisture concentration $c\,[kg/m^3]$:

$$W_c = \int_V c\, dV\,, \tag{10}$$

the mass of the dry material is obtained by means of the integration in the volume V of the mass density of the dry material $\rho_d\,[kg/m^3]$:

$$W_d = \int_V \rho_d\, dV\,. \tag{11}$$

Opportunely combining Eqs.(9)-(11), the moisture content can be also written as:

$$\mathcal{M}(\%) = \frac{c\,V}{\rho_d\,V} \times (100) = \frac{c}{\rho_d} \times (100)\,, \tag{12}$$

the moisture concentration c is defined as $[kg/m^3]$, the moisture content $\mathcal{M}$ has a no-dimensional form because it is obtained from c divided for the mass density of the dry material ρ_d. When the moisture content $\mathcal{M}$ is given in non-dimensional form $[-]$, the related moisture expansion coefficients η_i must be given in non-dimensional form $[-]$ too. If the moisture content $\mathcal{M}$ is expressed in percentage %, the related moisture expansion coefficients η_i are proposed as $[\frac{1}{\%}]$.

The compact matrix form of the constitutive equations is:

$$\boldsymbol{\sigma}^k = \boldsymbol{C}^k \boldsymbol{\epsilon}^k = \boldsymbol{C}^k (\boldsymbol{\epsilon}_m^k - \boldsymbol{\epsilon}_{\mathcal{M}}^k)\,, \tag{13}$$

where $\boldsymbol{\sigma}^k$ is the 6×1 stress vector, $\boldsymbol{C}^k$ is the 6×6 elastic coefficient matrix and the strains have been already defined in details in Eqs.(1)-(6). In order to obtain closed form solutions, orthotropic angles must be 0° or 90° to consider $C_{16}^k = C_{26}^k = C_{36}^k = C_{45}^k = 0$. Therefore, the elastic coefficient matrix in the structural reference system (α, β, z) is:

$$\boldsymbol{C}^k = \begin{bmatrix} C_{11}^k & C_{12}^k & C_{13}^k & 0 & 0 & 0 \\ C_{12}^k & C_{22}^k & C_{23}^k & 0 & 0 & 0 \\ C_{13}^k & C_{23}^k & C_{33}^k & 0 & 0 & 0 \\ 0 & 0 & 0 & C_{44}^k & 0 & 0 \\ 0 & 0 & 0 & 0 & C_{55}^k & 0 \\ 0 & 0 & 0 & 0 & 0 & C_{66}^k \end{bmatrix}. \tag{14}$$

The substitution of geometrical equations (1)-(6) in the constitutive equation (13) gives the following

relations:

$$\sigma^k_{\alpha\alpha} = \frac{C^k_{11}}{H_\alpha}u^k_{,\alpha} + \frac{C^k_{11}}{H_\alpha R_\alpha}w^k + \frac{C^k_{12}}{H_\beta}v^k_{,\beta} + \frac{C^k_{12}}{H_\beta R_\beta}w^k + C^k_{13}w^k_{,z} - \xi^k_\alpha \mathcal{M}^k \,, \tag{15}$$

$$\sigma^k_{\beta\beta} = \frac{C^k_{12}}{H_\alpha}u^k_{,\alpha} + \frac{C^k_{12}}{H_\alpha R_\alpha}w^k + \frac{C^k_{22}}{H_\beta}v^k_{,\beta} + \frac{C^k_{22}}{H_\beta R_\beta}w^k + C^k_{23}w^k_{,z} - \xi^k_\beta \mathcal{M}^k \,, \tag{16}$$

$$\sigma^k_{zz} = \frac{C^k_{13}}{H_\alpha}u^k_{,\alpha} + \frac{C^k_{13}}{H_\alpha R_\alpha}w^k + \frac{C^k_{23}}{H_\beta}v^k_{,\beta} + \frac{C^k_{23}}{H_\beta R_\beta}w^k + C^k_{33}w^k_{,z} - \xi^k_z \mathcal{M}^k \,, \tag{17}$$

$$\sigma^k_{\beta z} = \frac{C^k_{44}}{H_\beta}w^k_{,\beta} + C^k_{44}v^k_{,z} - \frac{C^k_{44}}{H_\beta R_\beta}v^k \,, \tag{18}$$

$$\sigma^k_{\alpha z} = \frac{C^k_{55}}{H_\alpha}w^k_{,\alpha} + C^k_{55}u^k_{,z} - \frac{C^k_{55}}{H_\alpha R_\alpha}u^k \,, \tag{19}$$

$$\sigma^k_{\alpha\beta} = \frac{C^k_{66}}{H_\alpha}v^k_{,\alpha} + \frac{C^k_{66}}{H_\beta}u^k_{,\beta} \,, \tag{20}$$

subscripts $(,\alpha)$, $(,\beta)$ and $(,z)$ means partial derivatives $(\frac{\partial}{\partial\alpha})$, $(\frac{\partial}{\partial\beta})$ and $(\frac{\partial}{\partial z})$, respectively. The hygro-mechanical coupling coefficients ξ^k_α, ξ^k_β and ξ^k_z in Eqs.(15)-(20) defined in the structural reference system (α, β, z) have the following form:

$$\xi^k_\alpha = C^k_{11}\eta^k_\alpha + C^k_{12}\eta^k_\beta + C^k_{13}\eta^k_z \,, \tag{21}$$

$$\xi^k_\beta = C^k_{12}\eta^k_\alpha + C^n_{22}\eta^k_\beta + C^k_{23}\eta^k_z \,, \tag{22}$$

$$\xi^k_z = C^k_{13}\eta^k_\alpha + C^n_{23}\eta^k_\beta + C^k_{33}\eta^k_z \,. \tag{23}$$

For a spherical shell (constant radii of curvature $R_\alpha = R_\beta$) with a total number N_L of physical k layers, the 3D equations of equilibrium are:

$$H_\beta\frac{\partial\sigma^k_{\alpha\alpha}}{\partial\alpha} + H_\alpha\frac{\partial\sigma^k_{\alpha\beta}}{\partial\beta} + H_\alpha H_\beta\frac{\partial\sigma^k_{\alpha z}}{\partial z} + (\frac{2H_\beta}{R_\alpha} + \frac{H_\alpha}{R_\beta})\sigma^k_{\alpha z} = 0, \tag{24}$$

$$H_\beta\frac{\partial\sigma^k_{\alpha\beta}}{\partial\alpha} + H_\alpha\frac{\partial\sigma^k_{\beta\beta}}{\partial\beta} + H_\alpha H_\beta\frac{\partial\sigma^k_{\beta z}}{\partial z} + (\frac{2H_\alpha}{R_\beta} + \frac{H_\beta}{R_\alpha})\sigma^k_{\beta z} = 0, \tag{25}$$

$$H_\beta\frac{\partial\sigma^k_{\alpha z}}{\partial\alpha} + H_\alpha\frac{\partial\sigma^k_{\beta z}}{\partial\beta} + H_\alpha H_\beta\frac{\partial\sigma^k_{zz}}{\partial z} - \frac{H_\beta}{R_\alpha}\sigma^k_{\alpha\alpha} - \frac{H_\alpha}{R_\beta}\sigma^k_{\beta\beta} + (\frac{H_\beta}{R_\alpha} + \frac{H_\alpha}{R_\beta})\sigma^k_{zz} = 0\,. \tag{26}$$

Eqs.(24)-(26) degenerate in those for cylinders and cylindrical panels when one of the two radii of curvature is infinite and in those for plates when both the radii of curvature are infinite.

The main hypothesis to obtain a closed-form solution for Eqs.(24)-(26) is simply supported sides for structures and consequent harmonic forms for displacement components and scalar moisture content:

$$u^k(\alpha,\beta,z) = U^k(z)cos(\bar\alpha\alpha)sin(\bar\beta\beta) \,, \tag{27}$$

$$v^k(\alpha,\beta,z) = V^k(z)sin(\bar\alpha\alpha)cos(\bar\beta\beta) \,, \tag{28}$$

$$w^k(\alpha,\beta,z) = W^k(z)sin(\bar\alpha\alpha)sin(\bar\beta\beta) \,, \tag{29}$$

$$\mathcal{M}^k(\alpha,\beta,z) = M^k(z)sin(\bar\alpha\alpha)sin(\bar\beta\beta) \,, \tag{30}$$

the two terms $\bar\alpha$ and $\bar\beta$ are calculated as $\bar\alpha = \frac{m\pi}{a}$ and $\bar\beta = \frac{n\pi}{b}$ where a and b are the in-plane structure dimensions referred to the mid-plane Ω_0. m and n are the half-wave numbers in in-plane directions. $U^k(z)$, $V^k(z)$ and $W^k(z)$ are the displacement amplitude components and $M^k(z)$ is the moisture content amplitude.

Harmonic forms for displacements and moisture content (see Eqs.(27)-(30)) and constitutive equations opportunely rearranged (see Eqs.(15)-(20)) are substituted in 3D equilibrium equations for spherical shells (see Eqs.(24)-(26)):

$$A_1^j U^j + A_2^j V^j + A_3^j W^j + A_4^j U^j_{,z} + A_5^j W^j_{,z} + A_6^j U^j_{,zz} + L_1^j M^j = 0 \,, \tag{31}$$

$$A_7^j U^j + A_8^j V^j + A_9^j W^j + A_{10}^j V^j_{,z} + A_{11}^j W^j_{,z} + A_{12}^j V^j_{,zz} + L_2^j M^j = 0 \,, \tag{32}$$

$$A_{13}^j U^j + A_{14}^j V^j + A_{15}^j W^j + A_{16}^j U^j_{,z} + A_{17}^j V^j_{,z} + A_{18}^j W^j_{,z} + A_{19}^j W^j_{,zz} + L_3^j M^j_{,z} + L_4^j M^j = 0 \,. \tag{33}$$

The Eqs.(31)-(33) are a system of three differential equations of second order in z. The involved terms are the displacement and moisture content amplitudes and the related derivatives performed with respect to z. The derivatives performed with respect to α and β coordinates have been exactly calculated thanks the use of harmonic forms. The proposed equations had not constant coefficients because the parametric coefficients H_α and H_β depend on z. Each k physical layer was divided in an appropriate number of mathematical layers defined by a new index j. This index j goes from 1 to the global number of mathematical layers G. In each j mathematical layer, the coefficients H_α and H_β can be exactly calculated via the use of the z coordinate in the middle of each j layer. In this way, coefficients A_s^j (with s from 1 to 19) and coefficients L_r^j (with r from 1 to 4) become constant terms in the compact form of the system of differential equations in z proposed in Eqs.(31)-(33); in them, the variables can be decoupled. Therefore, the moisture content profile through the thickness direction z will be separately calculated in the next section and it becomes a known term. As a consequence, the system will be a system of second order differential equations in the displacement amplitudes U^j, V^j, W^j and their derivatives in z. By using the methodology proposed in [64] and [65] and based on the redoubling of variables, the system is reduced to a first order differential equation system in z. In each j layer, the variables pass from 3 (U^j, V^j, W^j) to 6 (U^j, V^j, W^j, $U^{j'}$, $V^{j'}$, $W^{j'}$) where superscript $'$ means derivatives performed with respect to z (also indicated as $\frac{\partial}{\partial z}$). Terms M^j and $M^{j'}$ are known terms because they can be calculated using one of the three different methods proposed in the next section 3:

$$\begin{bmatrix} A_6^j & 0 & 0 & 0 & 0 & 0 \\ 0 & A_{12}^j & 0 & 0 & 0 & 0 \\ 0 & 0 & A_{19}^j & 0 & 0 & 0 \\ 0 & 0 & 0 & A_6^j & 0 & 0 \\ 0 & 0 & 0 & 0 & A_{12}^j & 0 \\ 0 & 0 & 0 & 0 & 0 & A_{19}^j \end{bmatrix} \begin{bmatrix} U^j \\ V^j \\ W^j \\ U^{j'} \\ V^{j'} \\ W^{j'} \end{bmatrix}' =$$

$$\begin{bmatrix} 0 & 0 & 0 & A_6^j & 0 & 0 \\ 0 & 0 & 0 & 0 & A_{12}^j & 0 \\ 0 & 0 & 0 & 0 & 0 & A_{19}^j \\ -A_1^j & -A_2^j & -A_3^j & -A_4^j & 0 & -A_5^j \\ -A_7^j & -A_8^j & -A_9^j & 0 & -A_{10}^j & -A_{11}^j \\ -A_{13}^j & -A_{14}^j & -A_{15}^j & -A_{16}^j & -A_{17}^j & -A_{18}^j \end{bmatrix} \begin{bmatrix} U^j \\ V^j \\ W^j \\ U^{j'} \\ V^{j'} \\ W^{j'} \end{bmatrix} + \begin{bmatrix} 0 & 0 & 0 & 0 & 0 & 0 \\ 0 & 0 & 0 & 0 & 0 & 0 \\ 0 & 0 & 0 & 0 & 0 & 0 \\ -L_1^j & 0 & 0 & 0 & 0 & 0 \\ -L_2^j & 0 & 0 & 0 & 0 & 0 \\ -L_4^j & -L_3^j & 0 & 0 & 0 & 0 \end{bmatrix} \begin{bmatrix} M^j \\ M^{j'} \\ 0 \\ 0 \\ 0 \\ 0 \end{bmatrix} , \tag{34}$$

A compact form of the above equation is:

$$\boldsymbol{D}^j \boldsymbol{U}^{j'} = \boldsymbol{A}^j \boldsymbol{U}^j + \boldsymbol{L}^j \boldsymbol{M}^j \,, \tag{35}$$

where the explicit forms of the various vectors are $\boldsymbol{U}^j = [U^j \; V^j \; W^j \; U^{j'} \; V^{j'} \; W^{j'}]^T$, $\boldsymbol{U}^{j'} = \frac{\partial \boldsymbol{U}^j}{\partial z}$ and $\boldsymbol{M}^j = [M^j \; M^{j'} \; 0 \; 0 \; 0 \; 0]^T$. T means the transpose of a vector. The Eq.(35) can be rearranged as:

$$\boldsymbol{U}^{j'} = \boldsymbol{D}^{j^{-1}} \boldsymbol{A}^j \boldsymbol{U}^j + \boldsymbol{D}^{j^{-1}} \boldsymbol{L}^j \boldsymbol{M}^j \,, \tag{36}$$

$$\boldsymbol{U}^{j'} = \boldsymbol{A}^{*j}\boldsymbol{U}^{j} + \boldsymbol{L}^{*j}\boldsymbol{M}^{j}\,, \tag{37}$$

where $\boldsymbol{A}^{*j} = \boldsymbol{D}^{j^{-1}}\boldsymbol{A}^{j}$ and $\boldsymbol{L}^{*j} = \boldsymbol{D}^{j^{-1}}\boldsymbol{L}^{j}$. After the calculation of the moisture content profile (using one of the three methodologies given in the next section 3), the actual profile can be reconstructed by means of linear approximations of the moisture content in each j mathematical layer. This approximation can be written as:

$$M^{j}(\tilde{z}^{j}) = a_{M}^{j}\tilde{z}^{j} + b_{M}^{j}\,, \tag{38}$$

where a_{M}^{j} and b_{M}^{j} are two constant terms in the j layer. The local thickness coordinate $\tilde{z}^{j}$ is opportunely defined and calculated for each j mathematical layer. $\tilde{z}^{j}$ goes from *0* at the bottom of the generic j layer to the thickness h^{j} of the same mathematical layer. The coefficients a_{M}^{j} and b_{M}^{j} will be calculated in each j layer as shown in the next section. Eq.(37) is a system of first order differential equations in $\tilde{z}$ or z; these equations are not homogeneous because of the hygroscopic term $\boldsymbol{L}^{*j}\boldsymbol{M}^{j}$ that depends on $\tilde{z}^{j}$ or z^{j}.

The exponential matrix method applied to a generic system of non-homogeneous first order differential equations considers the following steps:

$$\frac{\mathrm{d}\boldsymbol{x}}{\mathrm{d}t} = \boldsymbol{A}\boldsymbol{x} + \boldsymbol{f}(t)\,, \tag{39}$$

where $\boldsymbol{x}$ is a $G \times 1$ vector, $\boldsymbol{A}$ is a $G \times G$ matrix with constant coefficients and $\boldsymbol{f}(t) = [f_1(t) \dots f_G(t)]^T$ is a known function vector. A solution of the Eq. (39) can be:

$$\boldsymbol{x}(t) = \mathrm{e}^{\boldsymbol{A}(t-t_0)}\boldsymbol{x}_0 + \int_{t_0}^{t} \mathrm{e}^{\boldsymbol{A}(t-s)}\boldsymbol{f}(s)ds\,. \tag{40}$$

An explicit matrix form of the known term in Eq.(37) is:

$$\boldsymbol{M}^{*j} = \boldsymbol{L}^{*j}\boldsymbol{M}^{j} = \begin{bmatrix} 0 & 0 & 0 & 0 & 0 & 0 \\ 0 & 0 & 0 & 0 & 0 & 0 \\ 0 & 0 & 0 & 0 & 0 & 0 \\ -L_1^{*j} & 0 & 0 & 0 & 0 & 0 \\ -L_2^{*j} & 0 & 0 & 0 & 0 & 0 \\ -L_4^{*j} & -L_3^{*j} & 0 & 0 & 0 & 0 \end{bmatrix} \begin{bmatrix} a_M^j\tilde{z}^j + b_M^j \\ a_M^j \\ 0 \\ 0 \\ 0 \\ 0 \end{bmatrix} = \begin{bmatrix} 0 \\ 0 \\ 0 \\ -L_1^{*j}(a_M^j\tilde{z}^j + b_M^j) \\ -L_2^{*j}(a_M^j\tilde{z}^j + b_M^j) \\ -L_4^{*j}(a_M^j\tilde{z}^j + b_M^j) - L_3^{*j}a_M^j \end{bmatrix}. \tag{41}$$

Using the known term $\boldsymbol{M}^{*j}$, Eq. (37) can be written as:

$$\boldsymbol{U}^{j'} = \boldsymbol{A}^{*j}\boldsymbol{U}^{j} + \boldsymbol{M}^{*j}\,, \tag{42}$$

where $\boldsymbol{M}^{*j}$ contains only linear known functions in $\tilde{z}^{j}$. Therefore, the Eq. (42) can be solved as:

$$\boldsymbol{U}^{j}(\tilde{z}^{j}) = \mathrm{e}^{(\boldsymbol{A}^{*j}\tilde{z}^{j})}\boldsymbol{U}^{j}(0) + \int_{0}^{\tilde{z}^{j}} \mathrm{e}^{(\boldsymbol{A}^{*j}(\tilde{z}^{j}-s))}\boldsymbol{M}^{*j}(s)ds\,. \tag{43}$$

Terms $\boldsymbol{A}^{**j} = \mathrm{e}^{(\boldsymbol{A}^{*j}h^{j})}$ and $\boldsymbol{L}^{**j} = \int_0^{h^j} \mathrm{e}^{(\boldsymbol{A}^{*j}(h^{j}-s))}\boldsymbol{M}^{*j}(s)ds$ must be calculated in each j layer with thickness h^{j} in order to define the displacement vector at the top of each j mathematical layer. Therefore, the exponential matrix must be opportunely expanded and evaluated in each j layer having thickness h^{j}:

$$\boldsymbol{A}^{**j} = \mathrm{e}^{(\boldsymbol{A}^{*j}h^{j})} = \boldsymbol{I} + \boldsymbol{A}^{*j}h^{j} + \frac{\boldsymbol{A}^{*j\,2}}{2!}h^{j\,2} + \frac{\boldsymbol{A}^{*j\,3}}{3!}h^{j\,3} + \cdots + \frac{\boldsymbol{A}^{*j\,N}}{N!}h^{j\,N}\,, \tag{44}$$

where $\boldsymbol{I}$ is the 6×6 identity matrix. The integral shown in Eq.(43) can be evaluated in each j layer with thickness h^j by expanding the exponential matrix with the same methodology and the same order N already seen in Eq.(44):

$$\boldsymbol{L}^{**^j} = \int_0^{h^j} \mathrm{e}^{(\boldsymbol{A}^{*^j}(h^j-s))} \boldsymbol{M}^{*^j}(s)ds = \int_0^{h^j} \Big(\boldsymbol{I} + \boldsymbol{A}^{*^j}(h^j-s) + \frac{\boldsymbol{A}^{*^j\,2}}{2!}(h^j-s)^2 + \frac{\boldsymbol{A}^{*^j\,3}}{3!}(h^j-s)^3 + \cdots + \frac{\boldsymbol{A}^{*^j\,N}}{N!}(h^j-s)^N \Big) \boldsymbol{M}^{*^j}(s)ds \,. \tag{45}$$

The definitions of Eqs.(44) and (45) modify Eq.(43) as:

$$\boldsymbol{U}^j(h^j) = \boldsymbol{A}^{**^j}\boldsymbol{U}^j(0) + \boldsymbol{L}^{**^j} \,, \tag{46}$$

if $\boldsymbol{U}_t^j$ indicates $\boldsymbol{U}^j(h^j)$ and $\boldsymbol{U}_b^j$ indicates $\boldsymbol{U}^j(0)$ (t and b denote the top and bottom of each j layer, respectively), Eq.(46) is rewritten as:

$$\boldsymbol{U}_t^j = \boldsymbol{A}^{**^j}\boldsymbol{U}_b^j + \boldsymbol{L}^{**^j} \,. \tag{47}$$

Eq.(47) allows to link displacements and related derivatives in z defined at the top of the j mathematical layer with those defined at the bottom of the same j layer.

The proposed 3D shell model is based on a layer-wise approach, therefore inter-laminar continuity conditions in terms of displacements and transverse stresses must be enforced at each interface between the $j-1$ and the j layer. The interlaminar continuity conditions for displacements are:

$$u_b^j = u_t^{j-1} \,, \;\; v_b^j = v_t^{j-1} \,, \;\; w_b^j = w_t^{j-1} \,. \tag{48}$$

The inter-laminar continuity conditions for transverse shear and transverse normal stresses are:

$$\sigma_{zz_b}^j = \sigma_{zz_t}^{j-1} \,, \;\; \sigma_{\alpha z_b}^j = \sigma_{\alpha z_t}^{j-1} \,, \;\; \sigma_{\beta z_b}^j = \sigma_{\beta z_t}^{j-1} \,. \tag{49}$$

Eqs.(48) and (49) can be opportunely rewritten in displacement form by using the constitutive equations (15)-(20) and the harmonic form for the displacements and moisture content in eqs.(27)-(30). The methodology is the same already applied in [7]- [9] for the pure elastic analysis. For the hygro-elastic analysis, the continuity equation for the normal stress σ_{zz} has an additional hygroscopic term as shown by the coefficient T_{11} in the displacement form of Eqs.(48) and (49) that have been rewritten in matrix compact notation using two transfer matrices:

$$\begin{bmatrix} U \\ V \\ W \\ U' \\ V' \\ W' \end{bmatrix}_b^j = \begin{bmatrix} 1 & 0 & 0 & 0 & 0 & 0 \\ 0 & 1 & 0 & 0 & 0 & 0 \\ 0 & 0 & 1 & 0 & 0 & 0 \\ T_1 & 0 & T_2 & T_3 & 0 & 0 \\ 0 & T_4 & T_5 & 0 & T_6 & 0 \\ T_7 & T_8 & T_9 & 0 & 0 & T_{10} \end{bmatrix}^{j-1,j} \begin{bmatrix} U \\ V \\ W \\ U' \\ V' \\ W' \end{bmatrix}_t^{j-1} + \begin{bmatrix} 0 & 0 & 0 & 0 & 0 & 0 \\ 0 & 0 & 0 & 0 & 0 & 0 \\ 0 & 0 & 0 & 0 & 0 & 0 \\ 0 & 0 & 0 & 0 & 0 & 0 \\ 0 & 0 & 0 & 0 & 0 & 0 \\ T_{11} & 0 & 0 & 0 & 0 & 0 \end{bmatrix}^{j-1,j} \begin{bmatrix} M \\ M' \\ 0 \\ 0 \\ 0 \\ 0 \end{bmatrix}_t^{j-1} \,. \tag{50}$$

The portion including a diagonal of 1 represents displacement continuity of Eq.(48). Terms from T_1 to T_{11} represents the stress continuity of Eq.(49) given in terms of displacements and moisture content with the related derivatives in z. Eq.(50) can be compacted as:

$$\boldsymbol{U}_b^j = \boldsymbol{T}_U^{j-1,j}\boldsymbol{U}_t^{j-1} + \boldsymbol{T}_M^{j-1,j}\boldsymbol{M}_t^{j-1} \,. \tag{51}$$

Displacements and related derivatives in z defined at the bottom of the j layer are linked with displacements and moisture content (and their derivatives in z) calculated at the top of the (j-1) layer via the use of Eq.(51).

The investigated multilayered shells are simply supported, that means:

$$w = v = 0,\ \sigma_{\alpha\alpha} = 0 \quad \text{for} \quad \alpha = 0, a\,, \tag{52}$$

$$w = u = 0,\ \sigma_{\beta\beta} = 0 \quad \text{for} \quad \beta = 0, b \tag{53}$$

the above conditions are automatically satisfied by the use of harmonic forms for all the variables of the problem.

If the external surfaces of the multilayered shells are free stressed, this feature means that no mechanical loads are applied and $\sigma_{\alpha z} = \sigma_{\beta z} = \sigma_{zz} = 0$ at both external top and bottom surfaces. As already seen in [7]- [9], these conditions can be expressed in terms of displacements as:

$$\boldsymbol{B}_t^G \boldsymbol{U}_t^G = \boldsymbol{P}_t^G = \boldsymbol{0}\,, \tag{54}$$

$$\boldsymbol{B}_b^1 \boldsymbol{U}_b^1 = \boldsymbol{P}_b^1 = \boldsymbol{0}\,, \tag{55}$$

t and b indicates the top and bottom, respectively. Superscript G indicates the last mathematical layer and superscript 1 indicates the first layer. Vector $\boldsymbol{P} = (P_\alpha\, P_\beta\, P_z)^T$ contains the mechanical loads in the three directions α, β and z. It is imposed equals zero in the hygro-elastic analysis when the mechanical loads are absent and only the moisture content profile generates an equivalent load; otherwise, they contain several values different from zero in the case of application of mechanical load in the hygro-elastic evaluation. Matrices $\boldsymbol{B}$ allow the imposition of loads at the external surfaces of the shell, the explicit form of vectors $\boldsymbol{P}$ and $\boldsymbol{B}$ were shown in [7]- [9].

$\boldsymbol{U}_t^G = \boldsymbol{U}^G(h^G)$ can be written in relation with $\boldsymbol{U}_b^1 = \boldsymbol{U}^1(0)$ to obtain a matrix form for the algebraic system shown in Eqs.(54) and (55). This feature means that displacements and related derivatives in $\tilde{z}$ calculated at the top of the last layer are linked with those defined in $\tilde{z}$ at the bottom of the first layer, this condition is obtained by means of the recursively substitution of Eq.(51) into Eq.(47):

$$\begin{aligned}
\boldsymbol{U}_t^G = & \left(\boldsymbol{A}^{**G} \boldsymbol{T}_U^{G-1,G} \boldsymbol{A}^{**G-1} \boldsymbol{T}_U^{G-2,G-1} ..... \boldsymbol{A}^{**2} \boldsymbol{T}_U^{1,2} \boldsymbol{A}^{**1} \right) \boldsymbol{U}_b^1 + \\
& \Bigg(\boldsymbol{A}^{**G} \boldsymbol{T}_U^{G-1,G} \boldsymbol{A}^{**G-1} ..... \boldsymbol{A}^{**2} \boldsymbol{T}_U^{1,2} \boldsymbol{L}^{**1} + \\
& \boldsymbol{A}^{**G} \boldsymbol{T}_U^{G-1,G} \boldsymbol{A}^{**G-1} ..... \boldsymbol{A}^{**3} \boldsymbol{T}_U^{2,3} \boldsymbol{L}^{**2} + \\
& \vdots \\
& \boldsymbol{A}^{**G} \boldsymbol{T}_U^{G-1,G} \boldsymbol{L}^{**G-1} + \\
& \boldsymbol{L}^{**G} + \\
& \boldsymbol{A}^{**G} \boldsymbol{T}_U^{G-1,G} \boldsymbol{A}^{**G} ..... \boldsymbol{A}^{**2} \boldsymbol{T}_M^{1,2} \boldsymbol{M}_t^1 + \\
& \boldsymbol{A}^{**G} \boldsymbol{T}_U^{G-1,G} \boldsymbol{A}^{**G} ..... \boldsymbol{A}^{**3} \boldsymbol{T}_M^{2,3} \boldsymbol{M}_t^2 + \\
& \vdots \\
& \boldsymbol{A}^{**G} \boldsymbol{T}_U^{G-1,G} \boldsymbol{A}^{**G-1} \boldsymbol{T}_M^{G-2,G-1} \boldsymbol{M}_t^{G-2} + \\
& \boldsymbol{A}^{**G} \boldsymbol{T}_M^{G-1,G} \boldsymbol{M}_t^{G-1} \Bigg)\,.
\end{aligned} \tag{56}$$

The first block in Eq.(56) defined in parentheses is the 6×6 matrix $\boldsymbol{H}_m$ already seen for multilayered structures in [7]- [9] for the classical elastic analysis. In the case of hygro-elastic analysis, G terms including $\boldsymbol{L}^{**j}$ and $G-1$ terms including $\boldsymbol{M}_t^j$ are showed by Eq.(56): the first ones consider the

hygroscopic profile for each j mathematical layer, the second ones define the moisture content at each interface, the summation of all these terms are collected in parentheses of the second block and it defines the 6×1 vector $\boldsymbol{H}_M$:

$$\boldsymbol{U}_t^G = \boldsymbol{H}_m \boldsymbol{U}_b^1 + \boldsymbol{H}_M \,. \tag{57}$$

Eq.(54) can be defined in terms of $\boldsymbol{U}_b^1$ via the substitution of Eq.(57):

$$\boldsymbol{B}_t^G \boldsymbol{H}_m \boldsymbol{U}_b^1 = -\boldsymbol{B}_t^G \boldsymbol{H}_M \,. \tag{58}$$

Therefore, Eqs.(58) and (55) are grouped in:

$$\boldsymbol{E}\boldsymbol{U}_b^1 = \boldsymbol{P}_M \,, \tag{59}$$

where

$$\boldsymbol{E} = \begin{bmatrix} \boldsymbol{B}_t^G \boldsymbol{H}_m \\ \boldsymbol{B}_b^1 \end{bmatrix} \tag{60}$$

and

$$\boldsymbol{P}_M = \begin{bmatrix} -\boldsymbol{B}_t^G \boldsymbol{H}_M \\ \boldsymbol{0} \end{bmatrix} . \tag{61}$$

The showed method uses a layer wise approach: even if a high number of G mathematical layers are employed, the dimension of the $\boldsymbol{E}$ matrix always remains 6×6. The $\boldsymbol{E}$ matrix is the same already obtained for the pure elastic analysis in [7]- [9]. The difference is the addition of the load vector $\boldsymbol{P}_M$ that includes the equivalent hygroscopic loads. The final system in Eq.(59) formally does not change with respect to the pure elastic analysis, the only difference is in the hygroscopic field through the thickness that has been converted in an equivalent load $\boldsymbol{P}_M$ with dimension 6×1. Vector $\boldsymbol{P}$ can be added in the case of mechanical load application. The bottom displacement components and their derivatives in z are obtained from Eq.(59), displacement components and their derivatives in z are calculated at each thickness coordinate along the z direction of the multilayered structure thanks the use of Eqs.(51) and (47).

3 Moisture diffusion problem

As discussed in the previous section, the decoupling between the elastic and the hygrometric field requests to separately calculate the moisture content profile through the thickness direction of the entire multilayered shell. The considered structure is subjected to a moisture content field in harmonic form in the in-plane directions by assuming steady state conditions ($\frac{\partial \mathcal{M}}{\partial t} = 0$); this field is imposed at the external surfaces in terms of given amplitudes M_t at the top and M_b at the bottom. Using these conditions, the moisture content profile trough the thickness direction can be defined via three different methodologies in analogy with the methods already explained in [13] and [14] for the temperature field: the 3D version of the Fick diffusion law can be solved in analogy with the 3D Fourier heat conduction equation and the model is called as 3D($\mathcal{M}_c$,3D), the 1D version of the Fick diffusion law can be solved in the same way already seen for the 1D Fourier heat conduction equation and the obtained hygro-elastic shell model is called as 3D($\mathcal{M}_c$,1D); moreover, "a priori" linear assumed moisture content profile through the global thickness of the entire multilayered shell gives a hygro-elastic shell model named as 3D($\mathcal{M}_a$).

In the employed acronyms for the 3D shell hygro-elastic models, the term 3D outside the parentheses indicates that the elastic part of the model is based on the 3D shell model above detailed, the terms inside the parentheses indicate the methodology employed to define the moisture content profile through the thickness direction: the subscript c means that the moisture content $\mathcal{M}$ has been calculated via the 3D version or the 1D version of the Fick diffusion law, the subscript a means that the moisture content $\mathcal{M}$ has been "a priori" linearly assumed.

3.1 3D version of the Fick moisture diffusion equation

If we define a sort of moisture "flux" vector $\boldsymbol{g}$ in analogy with the heat flux vector $\boldsymbol{q}$ defined for the 3D version of the Fourier heat conduction equation, it is possible to write the differential equation of moisture diffusion, for a stationary case and a homogeneous solid without internal energy generation, in a general orthogonal curvilinear coordinate system (u_1, u_2, u_3) as:

$$\nabla \cdot \boldsymbol{g}(u_1, u_2, u_3) = 0\,. \tag{62}$$

If the coordinate system is orthogonal and curvilinear, the divergence of the moisture "flux" can be given as:

$$\nabla \cdot \boldsymbol{g} = \frac{1}{a}\left[\frac{\partial}{\partial u_1}\left(\frac{a}{a_1}g_1\right) + \frac{\partial}{\partial u_2}\left(\frac{a}{a_2}g_2\right) + \frac{\partial}{\partial u_3}\left(\frac{a}{a_3}g_3\right)\right], \tag{63}$$

where g_1, g_2, g_3 are the moisture "flux" components in 1, 2 and 3 directions, respectively:

$$g_i = -\mathcal{D}_i \frac{1}{a_i}\frac{\partial \mathcal{M}}{\partial u_i}\,, \tag{64}$$

where $\mathcal{D}_i$ are the diffusion coefficients in u_i directions. a_1, a_2 and a_3 are defined as scale factors and a is calculated as:

$$a = a_1\, a_2\, a_3\,. \tag{65}$$

Povstenko [66] demonstrated how Eq.(63) can be defined in a mixed curvilinear orthogonal coordinate system (α, β, z) in the case of orthotropic material as:

$$\frac{1}{H_\alpha H_\beta}\left[\frac{\partial}{\partial \alpha}\left(\frac{H_\alpha H_\beta}{H_\alpha}\mathcal{D}_1 \frac{1}{H_\alpha}\frac{\partial \mathcal{M}}{\partial \alpha}\right) + \frac{\partial}{\partial \beta}\left(\frac{H_\alpha H_\beta}{H_\beta}\mathcal{D}_2 \frac{1}{H_\beta}\frac{\partial \mathcal{M}}{\partial \beta}\right)\right] + \mathcal{D}_3 \frac{\partial^2 \mathcal{M}}{\partial z^2} = 0\ , \tag{66}$$

the Eq.(66) has been written by considering z as rectilinear and $H_z = 1$; the demonstration by Leissa [67] has been employed where the scale factors a_i can be replaced by the parametric coefficients as following:

$$a_1 = H_\alpha,\ a_2 = H_\beta,\ a_3 = H_z = 1\,. \tag{67}$$

The moisture "fluxes" have been already defined in Eqs.(63) and (64) using the analogy with the heat fluxes. Starting from Eq.(66), in the case of physical orthotropic layers k, the differential operators can be applied only on the moisture content in order to obtain:

$$\mathcal{D}_1^{*k}(z)\frac{\partial^2 \mathcal{M}}{\partial \alpha^2} + \mathcal{D}_2^{*k}(z)\frac{\partial^2 \mathcal{M}}{\partial \beta^2} + \mathcal{D}_3^{*k}(z)\frac{\partial^2 \mathcal{M}}{\partial z^2} = 0\,. \tag{68}$$

where

$$\mathcal{D}_1^{*k}(z) = \frac{\mathcal{D}_1^k}{H_\alpha^2}, \quad \mathcal{D}_2^{*k}(z) = \frac{\mathcal{D}_2^k}{H_\beta^2}, \quad \mathcal{D}_3^{*k}(z) = \mathcal{D}_3^k\,. \tag{69}$$

In the physical orthotropic k layer, the diffusion coefficients $\mathcal{D}_1^k$, $\mathcal{D}_2^k$ and $\mathcal{D}_3^k$ are defined in the material reference system. In Eq.(68), the coefficients are not constant in each k physical layer because in $\mathcal{D}_1^{*k}$ and $\mathcal{D}_2^{*k}$, H_α and H_β are functions of z. Therefore, the multilayered shell is divided into j mathematical layers in order to have G equations, one for each j mathematical layer, where the new coefficients $\mathcal{D}_1^{*j}$, $\mathcal{D}_2^{*j}$ and $\mathcal{D}_3^{*j}$ are now constant because terms H_α and H_β can be calculated in the middle of each j mathematical layer. Using this mathematical approximation, Eq.(68), that has not constant coefficients, can be rewritten as an equation with constant coefficients for each j layer:

$$\mathcal{D}_1^{*j}\frac{\partial^2 \mathcal{M}}{\partial \alpha^2} + \mathcal{D}_2^{*j}\frac{\partial^2 \mathcal{M}}{\partial \beta^2} + \mathcal{D}_3^{*j}\frac{\partial^2 \mathcal{M}}{\partial z^2} = 0\,. \tag{70}$$

The harmonic form for the moisture content $\mathcal{M}(\alpha,\beta,z)$ proposed in Eq.(30) automatically satisfies Eq.(70), the moisture content amplitude $M(z)$ has the following dependence on z:

$$M^j(z) = M_0^j \exp(s^j z)\,, \tag{71}$$

M_0^j and s^j must be defined in each j mathematical layer. s^j is determined via the substitution of Eq.(30) in Eq.(70) using the assumption shown in Eq.(71):

$$s_{1,2}^j = \pm\sqrt{\frac{\mathcal{D}_1^{*j}\bar{\alpha}^2 + \mathcal{D}_2^{*j}\bar{\beta}^2}{\mathcal{D}_3^{*j}}}\,, \tag{72}$$

the chosen solution is s_1^j by using the algebraic sign $+$. Therefore, Eq.(71) is modified in:

$$M^j(z) = M_{01}^j \exp(s_1^j z) + M_{02}^j \exp(s_1^j z)\,, \tag{73}$$

$$M^j(z) = S_1^j cosh(s_1^j z) + S_2^j sinh(s_1^j z)\,. \tag{74}$$

Eqs.(73) and (74) have constants that must be calculated in each j mathematical layer. s_1^j is determined via Eq.(72). Therefore, $2 \times G$ coefficients must be calculated. In order to obtain this result, two continuity conditions at each mathematical layer interface must be defined:

$$M_b^{(j+1)} = M_t^j\,, \tag{75}$$

$$\mathcal{D}_3^{*j+1} M_{,z_b}^{(j+1)} = \mathcal{D}_3^{*j} M_{,z_t}^j\,. \tag{76}$$

The moisture content at the top of the generic mathematical j layer is imposed equal to that at the bottom of the generic mathematical $j+1$ layer in Eq.(75). The moisture "flux" g_3 at the bottom of the generic mathematical $j+1$ layer is imposed equal to that at the top of the generic mathematical j layer in Eq.(76). S_1 and S_2 at the j layer and S_1 and S_2 at the $(j+1)$ layer are linked by means of a compact matrix form obtained from Eqs.(75) and (76) and using $M^j(z)$ as given in Eq.(74):

$$\begin{bmatrix} S_1 \\ S_2 \end{bmatrix}^{j+1} = \begin{bmatrix} V_{M_1}^{j+1,j} & V_{M_2}^{j+1,j} \\ V_{M_3}^{j+1,j} & V_{M_4}^{j+1,j} \end{bmatrix} \begin{bmatrix} S_1 \\ S_2 \end{bmatrix}^j\,. \tag{77}$$

$2 \times (G-1)$ conditions must be imposed where $(G-1)$ indicates the layer interfaces. $\boldsymbol{V}_M^{(j+1,j)}$ is the transfer matrix defined in Eq.(77). Therefore, coefficients at the top layer ($j = G$) and those at the bottom layer ($j = 1$) can be determined recursively by applying Eq.(77):

$$\begin{bmatrix} S_1 \\ S_2 \end{bmatrix}^G = \boldsymbol{V}_M^{(G,G-1)} \boldsymbol{V}_M^{(G-1,G-2)} ..... \boldsymbol{V}_M^{(3,2)} \boldsymbol{V}_M^{(2,1)} \begin{bmatrix} S_1 \\ S_2 \end{bmatrix}^1 = \boldsymbol{V}_M^{(G,1)} \begin{bmatrix} S_1 \\ S_2 \end{bmatrix}^1\,. \tag{78}$$

If the moisture contents at the bottom and at the top of the whole multilayered shell are correctly imposed, the 2 conditions missed in the $2 \times (G-1)$ conditions already imposed in Eq.(77) are correctly added and the problem proposed in Eq.(78) is now solvable. This feature means that all the $2 \times G$ coefficients can be determined: it means to calculate all the S_1^j and S_2^j for all the G mathematical layers. After the determination of the coefficients for the external layers, the other coefficients can be consequently and easily calculated.

As discussed in previous section, the implementation of this solution is not complicated if the moisture content is assumed as linear in each j mathematical layer. After the definition of the coefficients in Eq.(74) for each j mathematical layer, the moisture content profile through the entire thickness is totally determined. In this way, both the coefficients used in Eq.(38) can be calculated: b_M^j is the moisture content value at the bottom of the j layer, and a_M^j is the slope of the moisture content profile in the j layer. The 3D exact shell model developed in the previous section including this moisture content profile is called as 3D($\mathcal{M}_c$,3D).

3.2 1D version of the Fick moisture diffusion equation

The proposed problem is three-dimensional. However, when the plates or shells are thin (high thickness ratios a/h or R_α/h), the moisture content profile can be determined in a simpler way that considers only the material layer effect and not the thickness layer effect. The moisture content is completely defined in the $\alpha\beta$-plane via the harmonic form given in Eq.(30). The form of the three moisture "fluxes" in the k physical layer is:

$$g_1^k = \mathcal{D}_1^{*k}\bar{\alpha}M^k(z)cos(\bar{\alpha}\alpha)sin(\bar{\beta}\beta)\,, \tag{79}$$

$$g_2^k = \mathcal{D}_2^{*k}\bar{\beta}M^k(z)sin(\bar{\alpha}\alpha)cos(\bar{\beta}\beta)\,, \tag{80}$$

$$g_3^k = \mathcal{D}_3^{*k}M_{,z}^k(z)sin(\bar{\alpha}\alpha)sin(\bar{\beta}\beta)\,. \tag{81}$$

For thin structures and high thickness ratios, Eqs.(66) and (68) are simplified in:

$$\frac{\partial}{\partial z}\left(\mathcal{D}_3^*\frac{\partial M}{\partial z}\right) = 0\,, \tag{82}$$

where $\mathcal{D}_3^* = \mathcal{D}_3$ because z is a rectilinear coordinate. The moisture "fluxes" g_1 and g_2 can be discarded for high thickness ratios because $\bar{\alpha} = \frac{m\pi}{a}$ and $\bar{\beta} = \frac{m\pi}{b}$ are small. The term in parentheses in Eq. (82) is the moisture "flux" in the thickness $3 \equiv z$ direction for the whole multilayered structure. The meaning of Eq.(82) is that $g_3(z)$ can be assumed as constant in the thickness direction of the entire multilayered plate and shell:

$$g_3(z) = \left(\mathcal{D}_3^*\frac{\partial M}{\partial z}\right) = const. \tag{83}$$

Eq.(83) clearly indicates a constant moisture "flux" g_3 in the considered multilayered structure, and it is here employed to impose the continuity of moisture flux g_3 at each interface between two adjacent physical layers k or mathematical layers j. By considering a generic j mathematical layer, the differential operator in Eq.(83) can be written in an algebraic and simplified form where the slope of the moisture content profile is clearly indicate:

$$g_3^j = -\mathcal{D}_3^{*j}\frac{\partial M^j}{\partial z} = -\frac{\mathcal{D}_3^{*j}}{h^j}(M_t^j - M_b^j)\,. \tag{84}$$

The term $\mathcal{D}_3^{*j}/h^j$ can be defined in the j layer in analogy with the thermal conductance defined in [13] and [14]. The constant moisture "flux" through the thickness direction can be calculated using an equivalent resistance coefficient of the entire structure defined in analogy with the equivalent thermal resistance in [13] and [14] (that is based on the concept of electric resistance):

$$R_{z_{eq}} = \sum_{j=1}^{G}\frac{h^j}{\mathcal{D}_3^{*j}}\,. \tag{85}$$

After the definition of the equivalent resistance of the entire structure, the moisture flux g_3 for the entire plate or shell can be calculated by means of the definition of a single equivalent layer:

$$g_3 = -\frac{1}{R_{z_{eq}}}(M_t - M_b) = const. \tag{86}$$

where M_t and M_b are the applied moisture content amplitudes at the external surfaces of the entire structure. The moisture content at each z coordinate can be calculated by means of the continuity of g_3^j as defined in Eq.(84):

$$g_3^j = -\mathcal{D}_3^{*j}\frac{(M_t^j - M_b^j)}{h^j} = g_3^{j+1} = -\mathcal{D}_3^{*j+1}\frac{(M_t^{j+1} - M_b^{j+1})}{h^{j+1}} = g_3 = const.\,, \tag{87}$$

when the coefficient $\mathcal{D}_3^{*j}$ is different from a layer to another adjacent layer, the continuity of g_3^j is possible only if the slope of the moisture content profile $\frac{(M_t^j - M_b^j)}{h^j}$ also appropriately changes. This feature means that when the material of the layer changes, the slope of the moisture content profile also changes but remaining linear in the layer. For this reason, this 1D method allows to evaluate the material layer effect but not the thickness layer effect. Therefore, this methodology permits to consider only the stacking sequence and the material effects; this feature happens because 3D characteristics of the problem have been neglected and, as consequence, the related thickness layer effect. Therefore, this method is able to evaluate the change of diffusivity $\mathcal{D}_3^*$ in each layer and the related slope of the moisture content. The disadvantage is that the moisture content remains linear in each layer even if the layer is thick. The thickness layer effect (moisture content profile not linear in the thick layer) can only be evaluated by means of the use of the 3D version of Fick diffusion equation given in the previous subsection. As already discussed, the two coefficients of Eq.(38) (b_M^j and a_M^j) are the moisture content values at the bottom of the j layer and the related slope of the moisture content profile in it. The methodology described is the same for both the k physical and j mathematical layers. When the 3D exact shell model described in Section 2 uses the moisture content profile here calculated, the 3D($\mathcal{M}_c$,1D) shell model is employed.

3.3 Assumed linear moisture content profile

A further hypothesis to simplify the calculation of the moisture content profile is to also discard the material layer effect as well as the thickness layer effect. In this way, the moisture content profile is a priori assumed as linear through the entire thickness of the whole multilayered structure from the bottom to the top without including the change of the material for each layer. This simplification is very common in the literature but it is correct only if the shell is thin and embedding a single layer or several hygroscopically homogeneous layers. The coefficients necessary for Eq.(38) are calculated in the same way already seen in previous subsections. Moreover, the term a_M^j is even easier to be determined because it is the global slope of the moisture content profile for the whole multilayer structure. The 3D exact shell model developed in Section 2 combined with this assumed linear moisture content profile is called as 3D($\mathcal{M}_a$).

4 Results

This section proposes several results for the hygro-elastic analysis of single-layered and multilayered composite and sandwich plates and shells. It is organized in two main parts: the first part is devoted to the validation of the proposed and developed 3D shell hygro-elastic models, the second part shows new benchmarks in order to give several physical comments and to see the main differences between the three proposed moisture content profiles through the thickness direction.

In the preliminary validations, the proposed 3D shell hygro-elastic models are compared with well-known 3D elastic solutions from the literature in order to validate the elastic part of the developed 3D shell models; in these comparisons, some 3D FE models (built by means of Patran & Nastran) are also added. The validation of these 3D FE models is mandatory in order to develop some new assessments including the hygroscopic loads to also validate the hygroscopic part of the proposed 3D exact shell models. This step is necessary because in the literature there are not any 3D exact hygro-elastic models that can be used for comparison purposes. In the new proposed benchmarks, the developed and validated 3D shell models are employed without the hygroscopic part or including one of the three possible moisture content profiles in order to analyze composite and sandwich plates, cylinders, cylindrical shell panels and spherical shell panels. The effects of the presence of the hygroscopic load calculated in the three different ways are investigated for several geometries, thickness ratios, materials and lamination schemes.

4.1 Preliminary validations

The first assessment considers a simply-supported rectangular three-layered composite plate where a transverse normal mechanical load is applied at the top in harmonic form. The applied load has amplitude $P_{zt} = 1\,kPa$ and half-wave numbers $m = n = 1$. The in-plane dimensions of the plate are $a = 1\,m$ and $b = 3\,m$ with thickness ratios a/h equals 2, 4, 10, 20, 50 and 100. Each layer has thickness $h_1 = h_2 = h_3 = h/3$ and the lamination scheme is $0°/90°/0°$. The elastic properties of each carbon fibre composite layer are: Young moduli $E_1 = 172.37\,GPa$ and $E_2 = E_3 = 6.89476\,GPa$, Poisson ratios $\nu_{12} = \nu_{13} = \nu_{23} = 0.25$ and shear moduli $G_{12} = G_{13} = 3.4474\,GPa$ and $G_{23} = 1.3789\,GPa$. The reference solution is the 3D one proposed by Pagano in exact form for several plate configurations [62]. No-dimensional displacements $\bar{w} = w\frac{100E_2}{P_{zt}h(a/h)^4}$, no-dimensional in-plane normal stresses $\bar{\sigma}_{\alpha\alpha} = \sigma_{\alpha\alpha}\frac{1}{P_{zt}(a/h)^2}$ and no-dimensional transverse shear stresses $\bar{\sigma}_{\alpha z} = \sigma_{\alpha z}\frac{1}{P_{zt}(a/h)}$ at different thickness coordinates are proposed in Table 1 where the present 3D shell model is compared with the 3D solution by Pagano [62] and with a 3D FE solution obtained via Patran & Nastran using 3D HEX8 elements (typical 3D solid elements by Patran & Nastran with 8 nodes). The present 3D shell model is coincident with the 3D plate solution by Pagano for each thickness ratio and for each investigated variable when the order of expansion N for the exponential matrix is 3 and with a number of mathematical layers G equals 51. The 3D FE model always gives satisfactory results when 12 solid HEX8 elements are employed through the thickness direction and an appropriate number of elements is used in the in-plane directions. This assessment verifies that the proposed 3D exact shell model and the 3D FE model by Patran & Nastran correctly work for the mechanical analysis of multilayered anisotropic plates. Therefore, they result validated for such cases.

The second assessment aims to validate the proposed 3D exact shell solutions and the 3D FE model by Patran & Nastran when the previous assessment is extended to an hygroscopic stress analysis. Therefore, the plate is the same already described in the first assessment but the mechanical load is now replaced by an opportune imposition of a moisture content at the external surfaces in steady-state conditions. At the top of the plate the applied moisture content is $\mathcal{M}_t = 1.0\%$ and at the bottom it is $\mathcal{M}_b = 0.5\%$, the harmonic form uses half-wave numbers $m = n = 1$. The lamination scheme and the elastic properties do not change with respect to the first assessment. Moreover, the moisture expansion coefficients are $\eta_1 = 0\,\frac{1}{\%}$ and $\eta_2 = \eta_3 = 0.4 \times 10^{-2}\,\frac{1}{\%}$, and the diffusion coefficients are $\mathcal{D}_1 = 7.04\,\frac{kg}{ms}$ and $\mathcal{D}_2 = \mathcal{D}_3 = 4.96\,\frac{kg}{ms}$. The main results are proposed in Table 2 where displacements w and stresses $\sigma_{\alpha\alpha}$ and $\sigma_{\beta\beta}$ are given for different thickness ratios a/h. The 3D FE solution is obtained via the thermal stress analysis by Patran & Nastran using the analogy between thermal properties (temperature, thermal expansion coefficients and conductivity coefficients) and hygroscopic properties (moisture content, moisture expansion coefficients and diffusion coefficients). The 3D FE solutions are very close to results obtained via the 3D exact model when the moisture content profile is calculated via the solution of the 3D Fick diffusion law (3D($\mathcal{M}_c$,3D)). This feature is due to the fact that the thermal stress analysis via Patran & Nastran is performed by solving the 3D heat conduction problem and, in analogy, the hygroscopic stress analysis is evaluated by solving the 3D moisture diffusion problem. The 3D exact solution always gives satisfactory results (for each investigated variable and thickness ratio) when the order N is equal 3 and the number of mathematical layers G is at least equal to 51. The three 3D exact solutions are coincident for thin plates. For thick plates, the only correct results are those based on the 3D Fick diffusion law because they are able to consider the thickness layer effects. After this assessment, the 3D exact shell solution is validated for the hygroscopic stress analysis of plates.

The third assessment considers a simply supported cylindrical shell panel made of one single layer (having the same elastic properties seen in the assessment one) with fibre orientation equals $0°$. The load is applied in harmonic form at the top surface in the transverse normal direction as $P_{zt} = 6894.8\,GPa$ with half-wave numbers $m = 1$ and $n = 0$ (typical cylindrical bending problem). The radius of curvature in α direction is $R_\alpha = 10\,m$ and in β direction is infinite ($R_\beta = \infty$ means rectilinear side).

The in-plane dimensions are $a = \frac{\pi}{3} R_\alpha$ and $b = 100\, m$ and the investigated thickness ratios R_α/h are 2, 4, 10, 50, 100 and 500. Results in Table 3 are proposed as no-dimensional transverse normal displacement $\bar{w} = w \frac{10 E_2}{P_{zt} h (a/h)^4}$ and no-dimensional in-plane stress $\bar{\sigma}_{\alpha\alpha} = \sigma_{\alpha\alpha} \frac{1}{P_{zt}(a/h)^2}$. The reference solution is the 3D exact solution by Ren [63] opportunely developed for the cylindrical bending of cylindrical shell panels. The present 3D exact shell solution is always coincident with the reference one for each investigated variable and thickness ratio when the employed order of expansion is $N = 3$ and the number of mathematical layers G is at least equal to 50. The 3D FE model obtained with the use of the solid HEX8 elements of Patran & Nastran exhibits some difficulties for very thick structures but it is quite close to the two proposed 3D analytical solutions for moderately thick and thin shells. The comparisons proposed in Table 3 allow to validate the 3D exact shell model and the 3D FE solution in the case of pure elastic analysis of shells.

The fourth and last assessment considers the same shell geometry, lamination scheme and material properties already described in the third assessment. The elastic properties are those shown in the assessment one and the hygroscopic properties are those summarized in the assessment two. In this last case, the mechanical load is replaced by the application of a moisture content in steady-state conditions at the external surfaces: $\mathcal{M}_t = 1.0\%$ and $\mathcal{M}_b = 0.5\%$ in harmonic form with half-wave numbers $m = n = 1$. Table 4 proposes transverse normal displacement and in-plane normal stress for different thickness ratios. The 3D exact shell model employing a 3D calculated moisture content profile (3D($\mathcal{M}_c$,3D)) is mandatory in the case of thick shells. For moderately thin and thin shells, the 3D exact shell models employing a 3D calculated moisture content profile, a 1D calculated moisture content profile and a linear assumed moisture content profile are coincident because the material layer effect is not present in a one-layered structure but only the thickness layer effect is showed. All the 3D exact shell models give satisfactory results for order of expansion $N = 3$ and number of mathematical layers $G = 50$ (for each possible thickness ratio and for each investigated variable). The 3D FE model via Patran & Nastran gives satisfactory results when it uses 12 solid HEX8 elements through the thickness direction. The 3D FE model shows some difficulties for very thick shells even if it uses a 3D calculated moisture content profile through the thickness direction. This last assessment validates the 3D exact shell models in the case of curved structures when a moisture content profile is applied in steady state conditions.

The four proposed assessments allowed the validation of the proposed 3D shell models (3D calculated moisture content profile (3D($\mathcal{M}_c$,3D)), 1D calculated moisture content profile (3D($\mathcal{M}_c$,1D)) and linear assumed moisture content profile (3D($\mathcal{M}_a$))) for elastic and hygroscopic stress analysis of single- and multi-layered plates and shells. The comparisons were performed with well-known 3D elastic solutions already proposed in the literature for specific cases of plates or shells and/or with a 3D FE hygro-elastic model developed in Patran & Nastran. This choice has been performed because 3D exact solutions for hygro-elastic analyses were not found in the literature. After the proposed validation, the developed 3D shell models can be used with confidence to propose new benchmarks in order to analyze several effects in the hygro-elastic analysis of single- and multi-layered plates and shells.

4.2 Proposed benchmarks

All the proposed benchmarks always consider simply-supported structures and harmonic forms for moisture content profiles and mechanical loads in order to obtain exact solutions. Moreover, the moisture content analysis is developed in steady state conditions. In the previous assessments, it was demonstrated that the proposed 3D shell models always give satisfactory results for each possible case when $N = 3$ is employed as order of expansion for the exponential matrix and at least $G = 50$ mathematical layers are employed for the curvature approximation. In all the proposed benchmarks, the 3D shell models always use $N = 3$ and $G = 300$ in order to have the best possible solutions for each investigated case.

The first benchmark considers a five-layered sandwich square plate with imposed moisture contents at the external surfaces equal to $\mathcal{M}_t = 1.0\%$ and $\mathcal{M}_b = 0.0\%$ and transverse normal mechanical load applied at the top with amplitude $P_{zt} = 10\,kPa$ (all the harmonic forms have half-wave numbers $m = n = 1$). The in-plane plate dimensions are $a = b = 1\,m$ and the thickness ratios a/h goes from 2 (very thick plate) to 100 (thin plate). From the bottom to the top, the lamination scheme is $0°/90°/CORE/90°/0°$. The first two layers for the bottom sandwich skin and the last two layers for the top sandwich skin have thickness values $h_1 = h_2 = h_4 = h_5 = h/10$ where h is the total thickness of the plate. The thickness core is $h_3 = \frac{3}{5}h$. The core is a foam with the following elastic and hygroscopic properties: Young modulus $E = 3\,GPa$, Poisson ratio $\nu = 0.4$, moisture expansion coefficient $\eta = 0.28 \times 10^{-2}\,\frac{1}{\%}$ and diffusion coefficient $\mathcal{D} = 9.324 \times 10^{-8}\,\frac{kg}{ms}$. The skins are made of long fibre reinforced composite material with the following elastic and hygroscopic properties: Young moduli $E_1 = 138\,GPa$ and $E_2 = E_3 = 8.5\,GPa$, Poisson ratios $\nu_{12} = \nu_{13} = 0.29$ and $\nu_{23} = 0.36$, shear moduli $G_{12} = G_{13} = 4.5\,GPa$ and $G_{23} = 3.2\,GPa$, moisture expansion coefficients $\eta_1 = 0\,\frac{1}{\%}$ and $\eta_2 = \eta_3 = 0.4 \times 10^{-2}\,\frac{1}{\%}$, and diffusion coefficients $\mathcal{D}_1 = 7.04\,\frac{kg}{ms}$ and $\mathcal{D}_2 = \mathcal{D}_3 = 4.96\,\frac{kg}{ms}$. The main results are collected in Table 5 and in Figures 2 and 3. In Table 5, the 3D shell model is able to consider only the elastic part and the application of the mechanical load. The other three 3D shell models include the hygroscopic effects by means of three different moisture content profiles through the thickness: the 3D($\mathcal{M}_a$) considers a moisture content profile that is assumed a priori as linear through the thickness directions, the 3D($\mathcal{M}_c, 1D$) uses a calculated moisture content profile by solving the 1D moisture diffusion problem and the 3D($\mathcal{M}_c, 3D$) is based on a 3D moisture diffusion problem. When the hygroscopic effect is discarded (3D shell model), no moisture content is calculated and the results for displacements and stresses are completely different from those obtained via a hygroscopic-elastic 3D shell model. The 3D($\mathcal{M}_c, 3D$) shell model always gives the correct results for each thickness ratio and for each investigated variable because it is able to evaluate both thickness layer and material layer effects. The 3D($\mathcal{M}_c, 1D$) shell model is very close to the 3D($\mathcal{M}_c, 3D$) shell model only for thin structures because it is able to evaluate the material layer effect but it discards the thickness layer effect. The 3D($\mathcal{M}_a$) shell model always gives uncorrect results because the assumed linear temperature profile for the entire multilayered structure is not correct in the case of sandwich plates with high transverse anisotropy. These results are clearer thanks the observation of moisture content profiles through the thickness direction shown in Figure 2. In the case of thick sandwich plate, the only correct moisture content profile is the 3D calculated one because it considers the thickness layer effect (profile which is not linear inside each single thick layer) and the material layer effect (the slope of the moisture content profile changes passing from a layer to another layer because the material is different and the moisture diffusion coefficient also changes). The linear assumed moisture content profile is always rectilinear for the entire multilayered plate for both thick and thin cases. In the case of thin sandwich plate, the linear assumed moisture content profile remains uncorrect while the 1D and 3D calculated moisture content profiles are coincident because the thickness layer effect disappears: therefore, the profile is linear inside each single layer but its slope changes because of the use of different materials having different hygroscopic properties. The displacements shown in Figure 3 have the typical zigzag form of transversely anisotropic sandwich plates. The transverse normal stress σ_{zz} is continuous at each interface and it satisfies the external boundary loading conditions (0 at the bottom and $10\,kPa$ at the top). The in-plane stress $\sigma_{\alpha\alpha}$ and the transverse shear strain $\gamma_{\beta z}$ are discontinuous at each layer interface with the typical zigzag form due to the transverse anisotropy. Such figures demonstrate the correct implementation of the 3D shell model that uses a layer-wise approach for displacements and it obtains the derivatives of displacements in z directly from the model. These two features allow to correctly capture the zizag form of the variables and the interlaminar continuity of displacements and transverse shear/normal stresses.

The second benchmark proposes a three-layered composite cylindrical shell panel with lamination scheme $0°/90°/0°$. Each layer has thickness value equals $h_1 = h_2 = h_3 = \frac{h}{3}$. The shell dimensions are

$a = \frac{\pi}{3} R_\alpha$ and $b = 30\,m$ with radii of curvature $R_\alpha = 10\,m$ and $R_\beta = \infty$. The thickness ratios R_α/h vary from 4 to 500. A moisture content is imposed at the external surfaces with values $\mathcal{M}_t = 1.0\%$ and $\mathcal{M}_b = 0.5\%$ and half-wave numbers $m = n = 1$. The elastic and hygroscopic material properties are the same already seen for the composite skins employed in the benchmark one. Results in terms of displacements, strains and stresses are provided in Table 6, in this case the 3D elastic shell model is not employed because there is not any mechanical load. The differences between the three different shell models are due to the moisture content profiles through the thickness directions and they are clearer in the images proposed in Figure 4 where assumed linear, 1D calculated and 3D calculated moisture content profiles are compared for thin and thick shells. In these cases, the only effect is that linked with the thickness layer; the material layer effect is not visible with respect to the sandwich case because the diffusivity coefficients $\mathcal{D}_1^j$ and $\mathcal{D}_2^j$ are exchanged when the orthotropic angle passes from 0° to 90° while the $\mathcal{D}_3^j$ coefficient remains the same for all the layers. Therefore, for thin shells the three moisture content profiles are coincident because also the thickness layer effect disappears. Figure 5 shows displacements, stresses and strains trough the thickness of a thick shell obtained via a $3\mathrm{D}(\mathcal{M}_c, 3D)$ model. The typical affects of multilayered composite shells are shown: zigzag form of displacements, stresses and strains, interlaminar continuity of displacements and transverse normal/shear stresses and interlaminar discontinuity for in-plane stresses and for strains. These effects are correctly recovered because the 3D shell model uses a layer-wise approach and it correctly calculates the derivatives in z of all the displacement components.

The third benchmark is based on the analysis of a four-layered composite closed cylinder with lamination scheme $0^\circ/90^\circ/0^\circ/90^\circ$ and elastic and hygroscopic material properties already employed in benchmark two and also in the skins of benchmark one. The layers have all the same thickness $h_1 = h_2 = h_3 = h_4 = \frac{h}{4}$, and the thickness ratios R_α/h vary from 4 to 500. The cylinder geometry has dimensions $a = 2\pi R_\alpha$ and $b = 30\,m$ with radii of curvature $R_\alpha = 10\,m$ and $R_\beta = \infty$. No mechanical loads are applied, in fact the 3D pure elastic shell model is not proposed in Table 7, and the moisture content is imposed at the external surfaces as $\mathcal{M}_t = 1.0\%$ and $\mathcal{M}_b = 0.5\%$ with half-wave numbers $m = 2$ and $n = 1$. The meaning of the results proposed in Table 7 and in Figures 6 and 7 are very similar to those already discussed for benchmark two. Also the explanations for these results have been already discussed in the previous benchmark. The thickness layer effect in the moisture content profile trough the thickness shown in Figure 6 is now less pronounced than the benchmark two because of the circular simmetry of the closed cylinder. All the other considerations remain the same alrady given for the open cylindrical shell panel.

The fourth and last benchmark proposes a composite three-layered spherical shell panel with lamination scheme $0^\circ/90^\circ/0^\circ$. The composite material is the same already proposed in benchmarks two and three. Each layer has always the same thickness ($h_1 = h_2 = h_3 = \frac{h}{3}$). The in-plane dimensions are $a = b = \frac{\pi}{3} R_\alpha$ and the radii of curvature are $R_\alpha = R_\beta = 10\,m$. The thickness ratios R_α/h change in a range between 4 and 500. Only a moisture content profile is applied with amplitudes at the external surfaces equal to $\mathcal{M}_t = 1.0\%$ and $\mathcal{M}_b = 0.5\%$ and half-wave numbers $m = n = 1$. The results in terms of moisture content, displacements, stresses and strains are given for several thickness ratios in Table 8. The material of each layer remains the same, the change of the orthotropic angle from 0° to 90° exchanges the diffusivity coefficients $\mathcal{D}_1^j$ with the $\mathcal{D}_2^j$, while $\mathcal{D}_3^j$ remains always the same. This feature means that no material layer effects are visible but the only effect is that due to the thickness layer. For these reasons, the three 3D shell models are coincident for thin shells (the thickness layer effect disappears) and the $3\mathrm{D}(\mathcal{M}_c, 3D)$ model gives different results for thick shells where the thickness layer effect is clear. These considerations are valid for all the results proposed in Table 8 and for the moisture content profiles shown in Figure 8. The evaluations of displacements, stresses and strains through the thickness are given in Figure 9 where the typical zizag form and interlaminar continuity characteristics of stresses and displacements can be again remarked thanks the use of a layer wise shell model that includes the correct calculation of the displacement derivatives in z.

5 Conclusions

The present paper proposes an exact 3D hygro-elastic shell model for the static analysis of simply-supported single-layered and multilayered composite and sandwich plates, cylinders, cylindrical shell panels and spherical shell panels. The proposed shell model is based on the 3D equilibrium equations written in orthogonal mixed curvilinear coordinates. The partial derivatives in the in-plane directions are exactly calculated by means of simply-supported side hypotheses and harmonic forms for the variables. The obtained system of partial differential equations in z is solved by means of the exponential matrix method for both the elastic and hygroscopic parts. The hygroscopic part is considered by including an opportune equivalent hygroscopic load (that can be added to the classical mechanical load) calculated via the appropriate definition of the moisture content profile trough the thickness direction. This profile can be calculated by solving the 3D version or the 1D version of the Fick moisture diffusion law or it can be a priori imposed as linear through the entire thickness of the multilayered structure. From the results, it is clear how the importance of the moisture content inclusion is bigger for thicker structures even if it cannot be discarded for thinner plates and shells. Moreover, the proposed results are correct when the elastic part of the 3D shell model is correctly developed and implemented. However, the model must be combined with an appropriate moisture content profile through the thickness direction in order to obtain a correct equivalent hygroscopic load. The use of a priori assumed linear moisture content profile through the thickness is correct only if the structure is thin and homogeneous. The calculation of the moisture content profile through the thickness direction via the 1D Fick moisture diffusion law is correct for multilayered structures with transverse anisotropy and small thickness values for the embedded layers. This feature is due to the fact that the 1D version of the Fick moisture diffusion law is able to consider the material layer effect (the slope of the moisture content profile varies from a layer to another layer when the related diffusion coefficient of the considered material changes) but it is not able to include the thickness layer effect (that means to have the moisture content profile different from the linear one when the considered layer is thick). In order to consider both thickness layer and material layer effects in the definition of the moisture content profile in a multilayered structure, the use of the 3D version of the Fick moisture diffusion law is mandatory. In this case, the slope of the profile changes going from a layer to another one including a different material and this profile does not have a linear evaluation when the thickness of the layer is large.

References

[1] H. Bouadi, Hygrothermal Effects on Complex Moduli of Composite Laminates. *Ph.D. Dissertation*, University of Florida, 1998.

[2] R. Vodicka, Accelerated Environmental Testing of Composite Materials. *DSTO-TR-0657, Published by DSTO Aeronautical and Maritime Research Laboratory*, Commonwealth of Australia, 1997.

[3] S. Tabrez, M. Mitra and S. Gopalakrishnan, Modeling of degraded composite beam due to moisture absorption for wave based detection, *CMES: Computer Modeling in Engineering & Sciences*, 22, 77-90, 2007.

[4] D. Gawin and L. Sanavia, A unified approach to numerical modeling of fully and partially saturated porous materials by considering air dissolved in water, *CMES: Computer Modeling in Engineering & Sciences*, 53, 255-302, 2009.

[5] S.W. Tsai, Composites Design. *Think Composites*, Dayton, OH (USA), 1986.

[6] J.N. Reddy, Mechanics of Laminated Composite Plates and Shells. Theory and Analysis. *Second Edition, CRC Press*, Boca Raton (Florida), 2004.

[7] S. Brischetto, Exact elasticity solution for natural frequencies of functionally graded simply-supported structures, *CMES: Computer Modeling in Engineering & Sciences*, 95, 391-430, 2013.

[8] S. Brischetto, An exact 3D solution for free vibrations of multilayered cross-ply composite and sandwich plates and shells, *International Journal of Applied Mechanics*, 6, 1450076, 2014.

[9] S. Brischetto, Exact three-dimensional static analysis of single- and multi-layered plates and shells, *Composites Part B*, 119, 230-252, 2017.

[10] A. Messina, Three Dimensional Free Vibration Analysis of Cross-Ply Laminated Plates Through 2D and Exact Models. *In: 3rd International Conference on Integrity, Reliability and Failure*; July 2009, p. 20-24. Porto (Portugal).

[11] K.P. Soldatos and J. Ye, Axisymmetric static and dynamic analysis of laminated hollow cylinders composed of monoclinic elastic layers, *Journal of Sound and Vibration*, 184, 245-259, 1995.

[12] J. Fan and J. Zhang, Analytical solutions for thick, doubly curved, laminated shells, *Journal of Engineering Mechanics*, 118, 1338-1356, 1992.

[13] S. Brischetto and R. Torre, Thermo-elastic analysis of multilayered plates and shells based on 1D and 3D heat conduction problems, *Composite Structures*, 206, 326-353, 2018.

[14] S. Brischetto and R. Torre, 3D shell model for the thermo-mechanical analysis of FGM structures via imposed and calculated temperature profiles, *Aerospace Science and Technology*, 85, 125-149, 2019.

[15] F. Tornabene and S. Brischetto, 3D capability of refined GDQ models for the bending analysis of composite and sandwich plates, spherical and doubly-curved shells, *Thin-Walled Structures*, 129, 94-124, 2018.

[16] S. Brischetto and F. Tornabene, Advanced GDQ models and 3D stress recovery in multilayered plates, spherical and double-curved panels subjected to transverse shear loads, *Composites Part B*, 146, 244-269, 2018.

[17] J.C. Monge, J.L. Mantari and R.A. Arciniega, Computational semi-analytical method for the 3D elasticity bending solution of laminated composite and sandwich doubly-curved shells, *Engineering Structures*, 221, 110938, 2020.

[18] J.C. Monge and J.L. Mantari, 3D elasticity numerical solution for the static behavior of FGM shells, *Engineering Structures*, 208, 110159, 2020.

[19] J.C. Monge and J.L. Mantari, Exact solution of thermo-mechanical analysis of laminated composite and sandwich doubly-curved shell, *Composite Structures*, 245, 112323, 2020.

[20] S. Brischetto, Hygrothermal loading effects in bending analysis of multilayered composite plates, *CMES: Computer Modeling in Engineering & Sciences*, 88, 367-417, 2012.

[21] S. Brischetto, Hygrothermoelastic analysis of multi-layered composite and sandwich shells, *Journal of Sandwich Structures and Materials*, 15, 168-202, 2013.

[22] R. Chiba and Y. Sugano, Transient hygrothermoelastic analysis of layered plates with one-dimensional temperature and moisture variations through the thickness, *Composite Structures*, 93, 2260-2268, 2011.

[23] M. Gigliotti, F. Jacquemin, J. Molimard and A. Vautrin, Modelling and experimental characterisation of hygrothermoelastic stress in polymer matrix composites, *Macromolecular Symposia*, 257, 199-210, 2007.

[24] M. Gigliotti, F. Jacquemin and A. Vautrin, Assessment of approximate models to evaluate transient and cyclical hygrothermoelastic stress in composite plates, *International Journal of Solids and Structures*, 44, 733-759, 2007.

[25] W. Hufenbach and L. Kroll, Stress analysis of notched anisotropic finite plates under mechanical and hygrothermal loads, *Archive of Applied Mechanics*, 69, 145-159, 1999.

[26] M. Khalil, E. Bakhiet and A. El-Zoghby, Optimum design of laminated composites subjected to hygrothermal residual stresses, *Proceedings of the Institution of Mechanical Engineers, Part L: Journal of Materials Design and Applications*, 215, 175-186, 2001.

[27] L.P. Kollár and J.M. Patterson, Composite cylindrical segments subjected to hygrothermal and mechanical loads, *International Journal of Solids and Structures*, 30, 2525-2545, 1993.

[28] H.-S. Shen, The effects of hygrothermal conditions on the postbuckling of shear deformable laminated cylindrical shells, *International Journal of Solids and Structures*, 38, 6357-6380, 2001.

[29] G.C. Sih, Transient hygrothermal stresses in plates with and without cavities, *Fibre Science and Technology*, 18, 181-201, 1983.

[30] C. Wüthrich, Thick-walled composite tubes under mechanical and hygrothermal loading, *Composites*, 23, 407-413, 1992.

[31] A.M. Zenkour, Hygro-thermo-mechanical effects on FGM plates resting on elastic foundations, *Composite Structures*, 93, 234-238, 2010.

[32] S.Y. Lee, C.J. Chou, J.L. Jang and J.S. Lin, Hygrothermal effects on the linear and nonlinear analysis of symmetric angle-ply laminated plates, *Composite Structures*, 21, 41-48, 1992.

[33] A.K. Upadhyay, R. Pandey and K.K. Shukla, Nonlinear flexural response of laminated composite plates under hygro-thermo-mechanical loading, *Communications in Nonlinear Science and Numerical Simulation*, 15, 2634-2650, 2010.

[34] T.I. Thinh and N.N Khoa, Modelling the Mechanical and Hygrothermal Behaviour of Composite Laminates Using a High-Order Displacement Formulation, *International colloquium in Mechanics of Solids, Fluids, Structures and Interactions*, Nhatrang (Vietnam), 2000.

[35] B. Boukert, A. Benkhedda, E.B. Adda, M. Khodjet-Kesba, Hygrothermal stresses analysis of thick composite plates using high order theory under a Fick concentration distribution, *Procedia Structural Integrity*, 17, 37-43, 2019.

[36] N. Joshi and A. Muliana, Deformation in viscoelastic sandwich composites subject to moisture diffusion, *Composite Structures*, 92, 254-264, 2010.

[37] M. Khoshbakht, M.W. Lin and J.B. Berman, Analysis of moisture-induced stresses in an FRP composites reinforced masonry structure, *Finite Elements in Analysis and Design*, 42, 414-429, 2006.

[38] C.K. Kundu and J.-H. Han, Vibration characteristics and snapping behaviour of hygro-thermo-elastic composite doubly curved shells, *Composite Structures*, 91, 306-317, 2009.

[39] C.K. Kundu and J.-H. Han, Nonlinear buckling analysis of hygrothermoelastic composite shell panels using finite element method, *Composite Part B*, 40, 313-328, 2009.

[40] S.P.C. Marques and G.J. Creus, Geometrically nonlinear finite element analysis of viscoelastic composite materials under mechanical and hygrothermal loads, *Computers and Structures*, 53, 449-456, 1994.

[41] N.V.S. Naidu and P.K. Sinha, Nonlinear finite element analysis of laminated composite shells in hygrothermal environments, *Composite Structures*, 69, 387-395, 2005.

[42] P.K. Parhi, S.K. Bhattacharyya and P.K. Sinha, Hygrothermal effects on the dynamic behavior of multiple delaminated composite plates and shells, *Journal of Sound and Vibration*, 248, 195-214, 2001.

[43] B.P. Patel, M. Ganapathi and D.P. Makhecha, Hygrothermal effects on the structural behaviour of thick composite laminates using higher-order theory, *Composite Structures*, 56, 25-34, 2002.

[44] K.S. Sai Ram and P.K. Sinha, Hygrothermal effects on the bending characteristics of laminated composite plates, *Computers and Structures*, 40, 1009-1015, 1991.

[45] K.S. Sai Ram and P.K. Sinha, Hygrothermal bending of laminated composite plates with a cutout, *Computers and Structures*, 43, 1105-1115, 1992.

[46] Z. Sereir, E.A. Adda-Bedia and A. Tounsi, Effect of temperature on the hygrothermal behaviour of unidirectional laminated plates with asymmetrical environmental conditions, *Composite Structures*, 72, 383-392, 2006.

[47] Z. Sereir, A. Tounsi and E.A. Adda-Bedia, Effect of the cyclic environmental conditions on the hygrothermal behavior of the symmetric hybrid composites, *Mechanics of Advanced Materials and Structures*, 13, 237-248, 2006.

[48] Z. Sereir, E.A. Adda-Bedia and N. Boualem, The evolution of transverse stresses in hybrid composites under hygrothermal loading, *Materials and Design*, 32, 3120-3126, 2001.

[49] A. Ghosh, Hygrothermal effects on the initiation and propagation of damage in composite shells, *Aircraft Engineering and Aerospace Technology: An International Journal*, 4, 386-399, 2008.

[50] S. Raja, P.K. Sinha, G. Prathap and D. Dwarakanathan, Influence of active stiffening on dynamic behaviour of piezo-hygro-thermo-elastic composite plates and shells, *Journal of Sound and Vibration*, 278, 257-283, 2004.

[51] A. Benkhedda, A. Tounsi and E.A. Adda-Bedia, Effect of temperature and humidity on transient hygrothermal stresses during moisture desorption in laminated composite plates, *Composite Structures*, 82, 629-635, 2008.

[52] A. Chateauminois, B. Chabert, J.P. Soulier and L. Vincent, Hygrothermal ageing effects on the static fatigue of glass/epoxy composites, *Composites*, 24, 547-555, 1993.

[53] S. Kellas, J. Morton and P.T. Curtis, The effect of hygrothermal environments upon the tensile and compressive strengths of notched CFRP laminates. Part 1: Static loading, *Composites*, 21, 41-51, 1990.

[54] L.K. Seng, T.T. Earn and V.P.W. Shim, Hygrothermal analysis of woven-fabric composite plates, *Composites Part B*, 28, 573-581, 1997.

[55] G.S. Springer, Moisture content of composites under transient conditions, *Journal of Composite Materials*, 11, 107-123, 1977.

[56] J.L. Abot, A. Yasmin and I.M. Daniel, Hygroscopic behavior of woven fabric carbon-epoxy composites, *Journal of Reinforced Plastics and Composites*, 24, 195-207, 2005.

[57] A. Szekeres, Analogy between heat and moisture thermo-hygro-mechanical tailoring of composites by taking into account the second sound phenomenon, *Computers and Structures*, 76, 145-152, 2000.

[58] A.A.O. Tay and K.Y. Goh, A Study of Delamination Growth in the Die-Attach Layer of Plastic IC Packages under Hygrothermal Loading During Solder Reflow, *49th Electronic Components and Technology Conference Proceedings*, 694-701, 1999.

[59] A.A.O. Tay and K.Y. Goh, A Study of delamination growth in the die-attach layer of plastic IC packages under hygrothermal loading during solder reflow, *IEEE Transactions on Device and Materials Reliability*, 3, 144-151, 2003.

[60] R. Di Domizio, A. Lupulescu and M.E. Glicksman, Simulation of Fick's Verification of the 2nd Law, *Journal for the Basic Principles of Diffusion Theory, Experiment and Application*, 4, 1-14, 2006.

[61] V. Tungikar and B.K.M. Rao, Three dimensional exact solution of thermal stresses in rectangular composite laminates, *Composite Structures*, 27, 419-439, 1994.

[62] N.J. Pagano, Exact solutions for rectangular bidirectional composites and sandwich plates, *Journal of Composite Materials*, 4, 20-34, 1970.

[63] J.G. Ren, Exact solutions for laminated cylindrical shells in cylindrical bending, *Composites Science and Technology*, 29, 169-187, 1987.

[64] W.E. Boyce and R.C. DiPrima, Elementary Differential Equations and Boundary Value Problems, John Wiley & Sons, Ltd., New York, 2001.

[65] Open document, Systems of Differential Equations, free available on http://www.math.utah.edu/gustafso/, accessed on 30th May 2013.

[66] Y. Povstenko, Fractional Thermoelasticity, Springer International Publishing, Switzerland, 2015.

[67] A.W. Leissa, Vibration of Shells, NASA SP-288, Washington D.C., USA, 1973.

G	3D	3D FE	Ref. [62]	3D	3D FE	Ref. [62]	3D	3D FE	Ref. [62]
$a/h = 2$									
	$\bar{w}$ at $\tilde{z} = h/2$			$\bar{\sigma}_{\alpha\alpha}$ at $\tilde{z} = 0$			$\bar{\sigma}_{\alpha z}$ at $\tilde{z} = h/2$		
21	8.17			-1.62			0.258		
51	8.17			-1.62			0.257		
102	8.17			-1.62			0.257		
150	8.17			-1.62			0.257		
201	8.17			-1.62			0.257		
300	8.17	8.16	8.17	-1.62	-1.60	-1.62	0.257	0.257	0.257
$a/h = 4$									
	$\bar{w}$ at $\tilde{z} = h/2$			$\bar{\sigma}_{\alpha\alpha}$ at $\tilde{z} = 0$			$\bar{\sigma}_{\alpha z}$ at $\tilde{z} = h/2$		
21	2.82			-1.10			0.352		
51	2.82			-1.10			0.351		
102	2.82			-1.10			0.351		
150	2.82			-1.10			0.351		
201	2.82			-1.10			0.351		
300	2.82	2.81	2.82	-1.10	-1.08	-1.10	0.351	0.350	0.351
$a/h = 10$									
	$\bar{w}$ at $\tilde{z} = h/2$			$\bar{\sigma}_{\alpha\alpha}$ at $\tilde{z} = 0$			$\bar{\sigma}_{\alpha z}$ at $\tilde{z} = h/2$		
21	0.919			-0.725			0.420		
51	0.919			-0.725			0.420		
102	0.919			-0.725			0.420		
150	0.919			-0.725			0.420		
201	0.919			-0.725			0.420		
300	0.919	0.913	0.919	-0.725	-0.716	-0.725	0.420	0.418	0.420
$a/h = 20$									
	$\bar{w}$ at $\tilde{z} = h/2$			$\bar{\sigma}_{\alpha\alpha}$ at $\tilde{z} = 0$			$\bar{\sigma}_{\alpha z}$ at $\tilde{z} = h/2$		
21	0.610			-0.650			0.434		
51	0.610			-0.650			0.434		
102	0.610			-0.650			0.434		
150	0.610			-0.650			0.434		
201	0.610			-0.650			0.434		
300	0.610	0.606	0.610	-0.650	-0.643	-0.650	0.434	0.431	0.434
$a/h = 50$									
	$\bar{w}$ at $\tilde{z} = h/2$			$\bar{\sigma}_{\alpha\alpha}$ at $\tilde{z} = 0$			$\bar{\sigma}_{\alpha z}$ at $\tilde{z} = h/2$		
21	0.520			-0.628			0.439		
51	0.520			-0.628			0.439		
102	0.520			-0.628			0.439		
150	0.520			-0.628			0.439		
201	0.520			-0.628			0.439		
300	0.520	0.519	0.520	-0.628	-0.622	-0.628	0.439	0.435	0.439
$a/h = 100$									
	$\bar{w}$ at $\tilde{z} = h/2$			$\bar{\sigma}_{\alpha\alpha}$ at $\tilde{z} = 0$			$\bar{\sigma}_{\alpha z}$ at $\tilde{z} = h/2$		
21	0.508			-0.624			0.439		
51	0.508			-0.624			0.439		
102	0.508			-0.624			0.439		
150	0.508			-0.624			0.439		
201	0.508			-0.624			0.439		
300	0.508	0.506	0.508	-0.624	-0.619	-0.624	0.439	0.436	0.439

Table 1: First assessment. $0°/90°/0°$ composite rectangular plate with an harmonic mechanical load applied at the top. Reference solution (Ref.) is the exact 3D solution by Pagano [62]. The proposed 3D model uses order N = 3 for the exponential matrix and different G mathematical layers.

G	3D($\mathcal{M}_a$)	3D($\mathcal{M}_c$,1D)	3D($\mathcal{M}_c$,3D)	3D FE	3D($\mathcal{M}_a$)	3D($\mathcal{M}_c$,1D)	3D($\mathcal{M}_c$,3D)	3D FE	3D($\mathcal{M}_a$)	3D($\mathcal{M}_c$,1D)	3D($\mathcal{M}_c$,3D)	3D FE
$a/h = 2$												
	w $[10^{-3}mm]$ at $\tilde{z} = h/2$				$\sigma_{\alpha\alpha}$ $[10^6 Pa]$ at $\tilde{z} = 0$				$\sigma_{\beta\beta}$ $[10^6 Pa]$ at $\tilde{z} = h$			
21	-0.0840	-0.0840	-0.0711		16.8	16.8	12.0		-12.2	-12.2	-12.5	
51	-0.0838	-0.0838	-0.0709		16.8	16.8	11.9		-12.2	-12.2	-12.5	
102	-0.0839	-0.0839	-0.0710		16.8	16.8	11.9		-12.2	-12.2	-12.5	
150	-0.0839	-0.0839	-0.0710		16.8	16.8	11.9		-12.2	-12.2	-12.5	
201	-0.0839	-0.0839	-0.0710		16.8	16.8	11.9		-12.2	-12.2	-12.5	
300	-0.0839	-0.0839	-0.0710	-0.0718	16.8	16.8	11.9	11.4	-12.2	-12.2	-12.5	-12.5
$a/h = 4$												
	w $[10^{-3}mm]$ at $\tilde{z} = h/2$				$\sigma_{\alpha\alpha}$ $[10^6 Pa]$ at $\tilde{z} = 0$				$\sigma_{\beta\beta}$ $[10^6 Pa]$ at $\tilde{z} = h$			
21	0.0125	0.0125	0.0135		7.88	7.88	7.06		-12.9	-12.9	-13.0	
51	0.0124	0.0124	0.0134		7.87	7.87	7.05		-12.9	-12.9	-13.0	
102	0.0124	0.0124	0.0133		7.87	7.87	7.05		-12.9	-12.9	-13.0	
150	0.0124	0.0124	0.0133		7.87	7.87	7.05		-12.9	-12.9	-13.0	
201	0.0124	0.0124	0.0133		7.87	7.87	7.05		-12.9	-12.9	-13.0	
300	0.0124	0.0124	0.0133	0.0114	7.87	7.87	7.05	6.89	-12.9	-12.9	-13.0	-13.0
$a/h = 10$												
	w $[10^{-3}mm]$ at $\tilde{z} = h/2$				$\sigma_{\alpha\alpha}$ $[10^6 Pa]$ at $\tilde{z} = 0$				$\sigma_{\beta\beta}$ $[10^6 Pa]$ at $\tilde{z} = h$			
21	0.0981	0.0981	0.0979		3.76	3.76	3.67		-13.2	-13.2	-13.2	
51	0.0980	0.0980	0.0978		3.76	3.76	3.67		-13.2	-13.2	-13.2	
102	0.0979	0.0979	0.0977		3.76	3.76	3.67		-13.2	-13.2	-13.2	
150	0.0979	0.0979	0.0977		3.76	3.76	3.67		-13.2	-13.2	-13.2	
201	0.0979	0.0979	0.0977		3.76	3.76	3.67		-13.2	-13.2	-13.2	
300	0.0979	0.0979	0.0977	0.0955	3.76	3.76	3.67	3.72	-13.2	-13.2	-13.2	-13.3
$a/h = 20$												
	w $[10^{-3}mm]$ at $\tilde{z} = h/2$				$\sigma_{\alpha\alpha}$ $[10^6 Pa]$ at $\tilde{z} = 0$				$\sigma_{\beta\beta}$ $[10^6 Pa]$ at $\tilde{z} = h$			
21	0.204	0.204	0.204		3.06	3.06	3.04		-13.3	-13.3	-13.3	
51	0.204	0.204	0.204		3.06	3.06	3.04		-13.3	-13.3	-13.3	
102	0.204	0.204	0.204		3.06	3.06	3.04		-13.3	-13.3	-13.3	
150	0.204	0.204	0.204		3.06	3.06	3.04		-13.3	-13.3	-13.3	
201	0.204	0.204	0.204		3.06	3.06	3.04		-13.3	-13.3	-13.3	
300	0.204	0.204	0.204	0.200	3.06	3.06	3.04	3.12	-13.3	-13.3	-13.3	-13.3
$a/h = 50$												
	w $[10^{-3}mm]$ at $\tilde{z} = h/2$				$\sigma_{\alpha\alpha}$ $[10^6 Pa]$ at $\tilde{z} = 0$				$\sigma_{\beta\beta}$ $[10^6 Pa]$ at $\tilde{z} = h$			
21	0.513	0.513	0.513		2.86	2.86	2.86		-13.3	-13.3	-13.3	
51	0.513	0.513	0.513		2.86	2.86	2.86		-13.3	-13.3	-13.3	
102	0.513	0.513	0.513		2.86	2.86	2.86		-13.3	-13.3	-13.3	
150	0.513	0.513	0.513		2.86	2.86	2.86		-13.3	-13.3	-13.3	
201	0.513	0.513	0.513		2.86	2.86	2.86		-13.3	-13.3	-13.3	
300	0.513	0.513	0.513	0.508	2.86	2.86	2.86	2.96	-13.3	-13.3	-13.3	-13.3
$a/h = 100$												
	w $[10^{-3}mm]$ at $\tilde{z} = h/2$				$\sigma_{\alpha\alpha}$ $[10^6 Pa]$ at $\tilde{z} = 0$				$\sigma_{\beta\beta}$ $[10^6 Pa]$ at $\tilde{z} = h$			
21	1.03	1.03	1.03		2.83	2.83	2.83		-13.3	-13.3	-13.3	
51	1.03	1.03	1.03		2.83	2.83	2.83		-13.3	-13.3	-13.3	
102	1.03	1.03	1.03		2.83	2.83	2.83		-13.3	-13.3	-13.3	
150	1.03	1.03	1.03		2.83	2.83	2.83		-13.3	-13.3	-13.3	
201	1.03	1.03	1.03		2.83	2.83	2.83		-13.3	-13.3	-13.3	
300	1.03	1.03	1.03	1.02	2.83	2.83	2.83	2.94	-13.3	-13.3	-13.3	-13.3

Table 2: Second assessment. $0°/90°/0°$ composite rectangular plate with applied moisture content at the external surfaces. The proposed 3D model uses order N = 3 for the exponential matrix and different G mathematical layers.

G	3D	3D FE	Ref. [63]	3D	3D FE	Ref. [63]	3D	3D FE	Ref. [63]
$R_\alpha/h = 2$									
	$\bar{w}$ at $\tilde{z} = h/2$			$\bar{\sigma}_{\alpha\alpha}$ at $\tilde{z} = 0$			$\bar{\sigma}_{\alpha\alpha}$ at $\tilde{z} = h$		
20	0.9976			-2.464			1.905		
50	0.9986			-2.456			1.907		
100	0.9986			-2.455			1.907		
150	0.9986			-2.455			1.907		
200	0.9986			-2.455			1.907		
300	0.9986	1.003	0.9986	-2.455	-2.368	-2.455	1.907	1.874	1.907
$R_\alpha/h = 4$									
	$\bar{w}$ at $\tilde{z} = h/2$			$\bar{\sigma}_{\alpha\alpha}$ at $\tilde{z} = 0$			$\bar{\sigma}_{\alpha\alpha}$ at $\tilde{z} = h$		
20	0.312			-1.332			1.078		
50	0.312			-1.331			1.078		
100	0.312			-1.331			1.079		
150	0.312			-1.331			1.079		
200	0.312			-1.331			1.079		
300	0.312	0.311	0.312	-1.331	-1.286	-1.331	1.079	1.050	1.079
$R_\alpha/h = 10$									
	$\bar{w}$ at $\tilde{z} = h/2$			$\bar{\sigma}_{\alpha\alpha}$ at $\tilde{z} = 0$			$\bar{\sigma}_{\alpha\alpha}$ at $\tilde{z} = h$		
20	0.115			-0.890			0.806		
50	0.115			-0.890			0.807		
100	0.115			-0.890			0.807		
150	0.115			-0.890			0.807		
200	0.115			-0.890			0.807		
300	0.115	0.113	0.115	-0.890	-0.867	-0.890	0.807	0.788	0.807
$R_\alpha/h = 50$									
	$\bar{w}$ at $\tilde{z} = h/2$			$\bar{\sigma}_{\alpha\alpha}$ at $\tilde{z} = 0$			$\bar{\sigma}_{\alpha\alpha}$ at $\tilde{z} = h$		
20	0.0770			-0.767			0.752		
50	0.0770			-0.767			0.752		
100	0.0770			-0.767			0.752		
150	0.0770			-0.767			0.752		
200	0.0770			-0.767			0.752		
300	0.0770	0.0764	0.0770	-0.767	-0.760	-0.767	0.752	0.746	0.752
$R_\alpha/h = 100$									
	$\bar{w}$ at $\tilde{z} = h/2$			$\bar{\sigma}_{\alpha\alpha}$ at $\tilde{z} = 0$			$\bar{\sigma}_{\alpha\alpha}$ at $\tilde{z} = h$		
20	0.0755			-0.758			0.751		
50	0.0755			-0.758			0.751		
100	0.0755			-0.758			0.751		
150	0.0755			-0.758			0.751		
200	0.0755			-0.758			0.751		
300	0.0755	0.0752	0.0755	-0.758	-0.753	-0.758	0.751	0.746	0.751
$R_\alpha/h = 500$									
	$\bar{w}$ at $\tilde{z} = h/2$			$\bar{\sigma}_{\alpha\alpha}$ at $\tilde{z} = 0$			$\bar{\sigma}_{\alpha\alpha}$ at $\tilde{z} = h$		
20	0.0749			-0.752			0.750		
50	0.0749			-0.752			0.750		
100	0.0749			-0.752			0.750		
150	0.0749			-0.752			0.750		
200	0.0749			-0.752			0.750		
300	0.0749	0.0745	0.0749	-0.752	-0.749	-0.752	0.750	0.747	0.750

Table 3: Third assessment. One-layered 0° cylindrical shell with an harmonic mechanical load applied at the top. Reference solution (Ref.) is the exact 3D solution by Ren [63]. The proposed 3D model uses order N = 3 for the exponential matrix and different G mathematical layers.

G	3D($\mathcal{M}_a$)	3D($\mathcal{M}_c$,1D)	3D($\mathcal{M}_c$,3D)	3D FE	3D($\mathcal{M}_a$)	3D($\mathcal{M}_c$,1D)	3D($\mathcal{M}_c$,3D)	3D FE	3D($\mathcal{M}_a$)	3D($\mathcal{M}_c$,1D)	3D($\mathcal{M}_c$,3D)	3D FE
					$Ra/h = 2$							
	w $[m]$ at $\tilde{z} = 0$				$\sigma_{\alpha\alpha}$ $[MPa]$ at $\tilde{z} = 0$				$\sigma_{\alpha\alpha}$ $[MPa]$ at $\tilde{z} = h$			
20	-0.00365	-0.00365	-0.00271		23.7	23.7	16.8		26.9	26.9	23.7	
50	-0.00365	-0.00365	-0.00271		23.6	23.6	16.8		26.9	26.9	23.8	
100	-0.00365	-0.00365	-0.00271		23.6	23.6	16.7		27.0	27.0	23.8	
150	-0.00365	-0.00365	-0.00271		23.6	23.6	16.7		27.0	27.0	23.8	
200	-0.00365	-0.00365	-0.00271		23.6	23.6	16.7		27.0	27.0	23.8	
300	-0.00365	-0.00365	-0.00271	-0.00266	23.6	23.6	16.7	16.2	27.0	27.0	23.8	22.0
					$Ra/h = 4$							
	w $[m]$ at $\tilde{z} = 0$				$\sigma_{\alpha\alpha}$ $[MPa]$ at $\tilde{z} = 0$				$\sigma_{\alpha\alpha}$ $[MPa]$ at $\tilde{z} = h$			
20	-0.00266	-0.00266	-0.00245		10.3	10.3	9.34		14.8	14.8	14.3	
50	-0.00266	-0.00266	-0.00245		10.3	10.3	9.32		14.8	14.8	14.3	
100	-0.00266	-0.00266	-0.00245		10.3	10.3	9.32		14.8	14.8	14.3	
150	-0.00266	-0.00266	-0.00245		10.3	10.3	9.32		14.8	14.8	14.3	
200	-0.00266	-0.00266	-0.00245		10.3	10.3	9.32		14.8	14.8	14.3	
300	-0.00266	-0.00266	-0.00245	-0.00239	10.3	10.3	9.32	8.98	14.8	14.8	14.3	13.8
					$Ra/h = 10$							
	w $[m]$ at $\tilde{z} = 0$				$\sigma_{\alpha\alpha}$ $[MPa]$ at $\tilde{z} = 0$				$\sigma_{\alpha\alpha}$ $[MPa]$ at $\tilde{z} = h$			
20	-0.00154	-0.00154	-0.00152		0.693	0.693	0.655		7.07	7.07	7.02	
50	-0.00154	-0.00154	-0.00152		0.693	0.693	0.654		7.08	7.08	7.03	
100	-0.00154	-0.00154	-0.00152		0.693	0.693	0.654		7.08	7.08	7.03	
150	-0.00154	-0.00154	-0.00152		0.693	0.693	0.654		7.08	7.08	7.03	
200	-0.00154	-0.00154	-0.00152		0.693	0.693	0.654		7.08	7.08	7.03	
300	-0.00154	-0.00154	-0.00152	-0.00144	0.693	0.693	0.654	0.447	7.08	7.08	7.03	6.28
					$Ra/h = 50$							
	w $[m]$ at $\tilde{z} = 0$				$\sigma_{\alpha\alpha}$ $[MPa]$ at $\tilde{z} = 0$				$\sigma_{\alpha\alpha}$ $[MPa]$ at $\tilde{z} = h$			
20	0.00823	0.00823	0.00823		-12.3	-12.3	-12.3		12.6	12.6	12.6	
50	0.00823	0.00823	0.00823		-12.3	-12.3	-12.3		12.6	12.6	12.6	
100	0.00823	0.00823	0.00823		-12.3	-12.3	-12.3		12.6	12.6	12.6	
150	0.00823	0.00823	0.00823		-12.3	-12.3	-12.3		12.6	12.6	12.6	
200	0.00823	0.00823	0.00823		-12.3	-12.3	-12.3		12.6	12.6	12.6	
300	0.00823	0.00823	0.00823	0.00810	-12.3	-12.3	-12.3	-10.5	12.6	12.6	12.6	10.4
					$Ra/h = 100$							
	w $[m]$ at $\tilde{z} = 0$				$\sigma_{\alpha\alpha}$ $[MPa]$ at $\tilde{z} = 0$				$\sigma_{\alpha\alpha}$ $[MPa]$ at $\tilde{z} = h$			
20	0.0326	0.0326	0.0326		-22.4	-22.4	-22.4		22.2	22.2	22.2	
50	0.0326	0.0326	0.0326		-22.4	-22.4	-22.4		22.2	22.2	22.2	
100	0.0326	0.0326	0.0326		-22.4	-22.4	-22.4		22.2	22.2	22.2	
150	0.0326	0.0326	0.0326		-22.4	-22.4	-22.4		22.2	22.2	22.2	
200	0.0326	0.0326	0.0326		-22.4	-22.4	-22.4		22.2	22.2	22.2	
300	0.0326	0.0326	0.0326	0.0329	-22.4	-22.4	-22.4	-18.5	22.2	22.2	22.2	16.8
					$Ra/h = 500$							
	w $[m]$ at $\tilde{z} = 0$				$\sigma_{\alpha\alpha}$ $[MPa]$ at $\tilde{z} = 0$				$\sigma_{\alpha\alpha}$ $[MPa]$ at $\tilde{z} = h$			
20	0.212	0.212	0.212		-28.2	-28.2	-28.2		28.1	28.1	28.1	
50	0.212	0.212	0.212		-28.2	-28.2	-28.2		28.1	28.1	28.1	
100	0.212	0.212	0.212		-28.2	-28.2	-28.2		28.1	28.1	28.1	
150	0.212	0.212	0.212		-28.2	-28.2	-28.2		28.1	28.1	28.1	
200	0.212	0.212	0.212		-28.2	-28.2	-28.2		28.1	28.1	28.1	
300	0.212	0.212	0.212	0.222	-28.2	-28.2	-28.2	-20.7	28.1	28.1	28.1	20.7

Table 4: Fourth assessment. One-layered 0° cylindrical shell with applied moisture content at the external surfaces. The proposed 3D model uses order N = 3 for the exponential matrix and different G mathematical layers.

a/h	2	4	10	50	100
$\mathcal{M}$ at $(\alpha = a/2, \beta = b/2; \tilde{z} = 4h/5)[-]$					
3D	-	-	-	-	-
3D($\mathcal{M}_a$)	0.8000	0.8000	0.8000	0.8000	0.8000
3D($\mathcal{M}_c, 1D$)	1.0000	1.0000	1.0000	1.0000	1.0000
3D($\mathcal{M}_c, 3D$)	0.8914	0.9709	0.9952	0.9998	1.0000
v at $(\alpha = a/2, \beta = 0; \tilde{z} = 4h/5)$ [10^{-2} mm]					
3D	0.006405	-0.004148	0.07625	-2.118	-8.495
3D($\mathcal{M}_a$)	-7.165	-9.489	-10.12	-12.11	-18.49
3D($\mathcal{M}_c, 1D$)	-7.759	-10.18	-10.90	-12.94	-19.31
3D($\mathcal{M}_c, 3D$)	-7.017	-9.879	-10.84	-12.93	-19.31
w at $(\alpha = a/2, \beta = b/2; \tilde{z} = h/2)$ [10^{-1} mm]					
3D	0.008901	0.02385	0.1367	11.51	90.69
3D($\mathcal{M}_a$)	-0.3691	0.7748	2.976	26.55	120.8
3D($\mathcal{M}_c, 1D$)	-1.043	0.6929	3.678	30.89	129.5
3D($\mathcal{M}_c, 3D$)	-0.8156	0.6990	3.667	30.88	129.5
σ_{zz} at $(\alpha = a/2, \beta = b/2; \tilde{z} = h/5)$ [10^{1} kPa]					
3D	0.1670	0.1460	0.1325	0.1298	0.1297
3D($\mathcal{M}_a$)	-95.33	-19.54	-2.631	0.02410	0.1033
3D($\mathcal{M}_c, 1D$)	-76.76	-15.07	-1.941	0.05121	0.1101
3D($\mathcal{M}_c, 3D$)	-55.91	-13.73	-1.908	0.05127	0.1101
$\sigma_{\alpha\alpha}$ at $(\alpha = a/2, \beta = b/2; \tilde{z} = h)$ [MPa]					
3D	0.05621	0.1220	0.6449	15.73	62.88
3D($\mathcal{M}_a$)	61.71	47.41	43.69	58.53	105.7
3D($\mathcal{M}_c, 1D$)	69.10	54.11	49.97	64.64	111.8
3D($\mathcal{M}_c, 3D$)	58.79	51.83	49.64	64.62	111.8
$\gamma_{\beta z}$ at $(\alpha = a/2, \beta = 0; \tilde{z} = h/3)$ [10^{-4}]					
3D	0.03317	0.06913	0.1688	0.8335	1.666
3D($\mathcal{M}_a$)	-15.18	-7.892	-3.402	0.06178	1.279
3D($\mathcal{M}_c, 1D$)	-16.93	-8.657	-3.628	0.02663	1.262
3D($\mathcal{M}_c, 3D$)	-12.67	-8.024	-3.586	0.02696	1.262

Table 5: First benchmark, sandwich square plate with imposed external moisture content and applied mechanical load. All the 3D solutions uses N=3 and G=300.

R_α/h	4	10	50	100	500
$\mathcal{M}$ at $(\alpha = a/2, \beta = b/2; \tilde{z} = h/2)[-]$					
3D($\mathcal{M}_a$)	0.7500	0.7500	0.7500	0.7500	0.7500
3D($\mathcal{M}_c, 1D$)	0.7500	0.7500	0.7500	0.7500	0.7500
3D($\mathcal{M}_c, 3D$)	0.6850	0.7389	0.7495	0.7499	0.7500
u at $(\alpha = 0, \beta = b/2; \tilde{z} = h/3)$ [mm]					
3D($\mathcal{M}_a$)	-1.643	-1.243	2.555	5.167	6.794
3D($\mathcal{M}_c, 1D$)	-1.643	-1.243	2.555	5.167	6.794
3D($\mathcal{M}_c, 3D$)	-1.514	-1.224	2.554	5.167	6.794
w at $(\alpha = a/2, \beta = b/2; \tilde{z} = h/2)$ [mm]					
3D($\mathcal{M}_a$)	-3.061	-2.621	8.252	16.11	21.17
3D($\mathcal{M}_c, 1D$)	-3.061	-2.621	8.252	16.11	21.17
3D($\mathcal{M}_c, 3D$)	-2.838	-2.582	8.249	16.11	21.17
σ_{zz} at $(\alpha = a/2, \beta = b/2; \tilde{z} = 2h/3)$ [MPa]					
3D($\mathcal{M}_a$)	-1.314	-0.5024	-0.1344	-0.06058	-0.007403
3D($\mathcal{M}_c, 1D$)	-1.314	-0.5024	-0.1344	-0.06058	-0.007403
3D($\mathcal{M}_c, 3D$)	-1.207	-0.4957	-0.1343	-0.06057	-0.007403
$\sigma_{\beta\beta}$ at $(\alpha = a/2, \beta = b/2; \tilde{z} = h)$ [MPa]					
3D($\mathcal{M}_a$)	-25.79	-26.27	-25.90	-25.73	-25.75
3D($\mathcal{M}_c, 1D$)	-25.79	-26.27	-25.90	-25.73	-25.75
3D($\mathcal{M}_c, 3D$)	-25.86	-26.28	-25.90	-25.73	-25.75
$\gamma_{\alpha\beta}$ at $(\alpha = 0, \beta = 0; \tilde{z} = 0)$ [10^{-3}]					
3D($\mathcal{M}_a$)	-1.026	-0.7063	-0.2706	-0.07889	0.01048
3D($\mathcal{M}_c, 1D$)	-1.026	-0.7063	-0.2706	-0.07889	0.01048
3D($\mathcal{M}_c, 3D$)	-0.9645	-0.6992	-0.2705	-0.07888	0.01048

Table 6: Second benchmark, three-layered composite cylindrical panel with imposed external moisture content. All the 3D solutions uses N=3 and G=300.

R_α/h	4	10	50	100	500
$\mathcal{M}$ at $(\alpha = a/2, \beta = b/2; \tilde{z} = h/2)[-]$					
3D($\mathcal{M}_a$)	0.7500	0.7500	0.7500	0.7500	0.7500
3D($\mathcal{M}_c, 1D$)	0.7500	0.7500	0.7500	0.7500	0.7500
3D($\mathcal{M}_c, 3D$)	0.7354	0.7476	0.7499	0.7500	0.7500
v at $(\alpha = a/2, \beta = 0; \tilde{z} = 3h/4)$ [mm]					
3D($\mathcal{M}_a$)	-1.133	-1.252	-1.281	-1.283	-1.284
3D($\mathcal{M}_c, 1D$)	-1.133	-1.252	-1.281	-1.283	-1.284
3D($\mathcal{M}_c, 3D$)	-1.117	-1.249	-1.281	-1.283	-1.284
w at $(\alpha = a/2, \beta = b/2; \tilde{z} = h/2)$ [mm]					
3D($\mathcal{M}_a$)	2.109	2.479	2.672	2.696	2.715
3D($\mathcal{M}_c, 1D$)	2.109	2.479	2.672	2.696	2.715
3D($\mathcal{M}_c, 3D$)	2.080	2.473	2.672	2.696	2.715
σ_{zz} at $(\alpha = a/2, \beta = b/2; \tilde{z} = h/4)$ [kPa]					
3D($\mathcal{M}_a$)	-680.9	172.3	95.63	51.54	10.90
3D($\mathcal{M}_c, 1D$)	-680.9	172.3	95.63	51.54	10.90
3D($\mathcal{M}_c, 3D$)	-664.4	172.2	95.62	51.54	10.90
$\sigma_{\alpha\beta}$ at $(\alpha = 0, \beta = 0; \tilde{z} = 0)$ [kPa]					
3D($\mathcal{M}_a$)	-703.8	-164.1	-24.90	-12.15	-2.389
3D($\mathcal{M}_c, 1D$)	-703.8	-164.1	-24.90	-12.15	-2.389
3D($\mathcal{M}_c, 3D$)	-692.9	-163.7	-24.90	-12.15	-2.389
$\gamma_{\beta z}$ at $(\alpha = a/2, \beta = 0; \tilde{z} = h/3)$ [10^{-5}]					
3D($\mathcal{M}_a$)	15.59	6.534	1.258	0.6243	0.1241
3D($\mathcal{M}_c, 1D$)	15.59	6.534	1.258	0.6243	0.1241
3D($\mathcal{M}_c, 3D$)	15.46	6.525	1.257	0.6243	0.1241

Table 7: Third benchmark, four-layered composite cylinder with imposed external moisture content. All the 3D solutions uses N=3 and G=300.

R_α/h	4	10	50	100	500
$\mathcal{M}$ at $(\alpha = a/2, \beta = b/2; \tilde{z} = h/2)[-]$					
3D($\mathcal{M}_a$)	0.7500	0.7500	0.7500	0.7500	0.7500
3D($\mathcal{M}_c, 1D$)	0.7500	0.7500	0.7500	0.7500	0.7500
3D($\mathcal{M}_c, 3D$)	0.6390	0.7301	0.7492	0.7498	0.7500
v at $(\alpha = a/2, \beta = 0; \tilde{z} = h/3)$ [mm]					
3D($\mathcal{M}_a$)	-0.8904	-0.6471	-0.2607	-0.2528	-0.2663
3D($\mathcal{M}_c, 1D$)	-0.8904	-0.6471	-0.2607	-0.2528	-0.2663
3D($\mathcal{M}_c, 3D$)	-0.7641	-0.6328	-0.2606	-0.2528	-0.2663
w at $(\alpha = a/2, \beta = b/2; \tilde{z} = h/2)$ [mm]					
3D($\mathcal{M}_a$)	-0.1617	0.3608	1.651	1.703	1.681
3D($\mathcal{M}_c, 1D$)	-0.1617	0.3608	1.651	1.703	1.681
3D($\mathcal{M}_c, 3D$)	0.05400	0.3680	1.650	1.703	1.681
σ_{zz} at $(\alpha = a/2, \beta = b/2; \tilde{z} = h/3)$ [kPa]					
3D($\mathcal{M}_a$)	-1080	-553.0	-59.78	-20.61	-2.559
3D($\mathcal{M}_c, 1D$)	-1080	-553.0	-59.78	-20.61	-2.559
3D($\mathcal{M}_c, 3D$)	-958.4	-544.2	-59.76	-20.60	-2.559
$\sigma_{\beta z}$ at $(\alpha = a/2, \beta = 0; \tilde{z} = 2h/3)$ [kPa]					
3D($\mathcal{M}_a$)	-4584	-2144	-463.4	-233.6	-46.95
3D($\mathcal{M}_c, 1D$)	-4584	-2144	-463.4	-233.6	-46.95
3D($\mathcal{M}_c, 3D$)	-4312	-2121	-463.1	-233.6	-46.95
$\epsilon_{\alpha\alpha}$ at $(\alpha = a/2, \beta = b/2; \tilde{z} = h)$ [10^{-4}]					
3D($\mathcal{M}_a$)	2.998	2.315	1.370	1.118	0.9025
3D($\mathcal{M}_c, 1D$)	2.998	2.315	1.370	1.118	0.9025
3D($\mathcal{M}_c, 3D$)	2.801	2.280	1.369	1.117	0.9025

Table 8: Fourth benchmark, three-layered composite spherical shell panel with imposed external moisture content. All the 3D solutions uses N=3 and G=300.

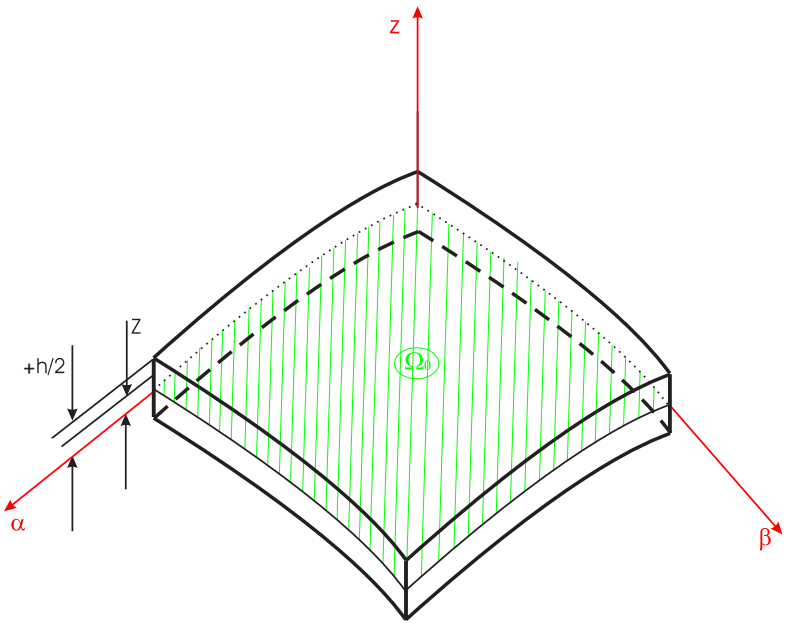

Figure 1: Shell geometry and related orthogonal mixed curvilinear coordinate system.

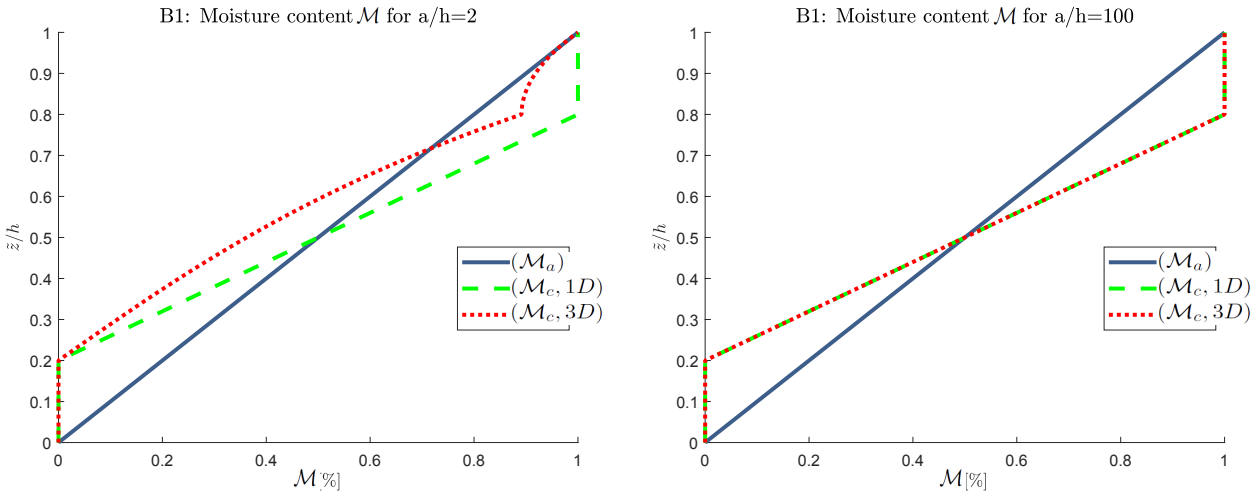

Figure 2: First benchmark, sandwich square plate with imposed external moisture content and applied mechanical load: moisture content profiles for thick (on the left) and thin (on the right) structure. The maximum moisture content is evaluated at $(a/2, b/2)$.

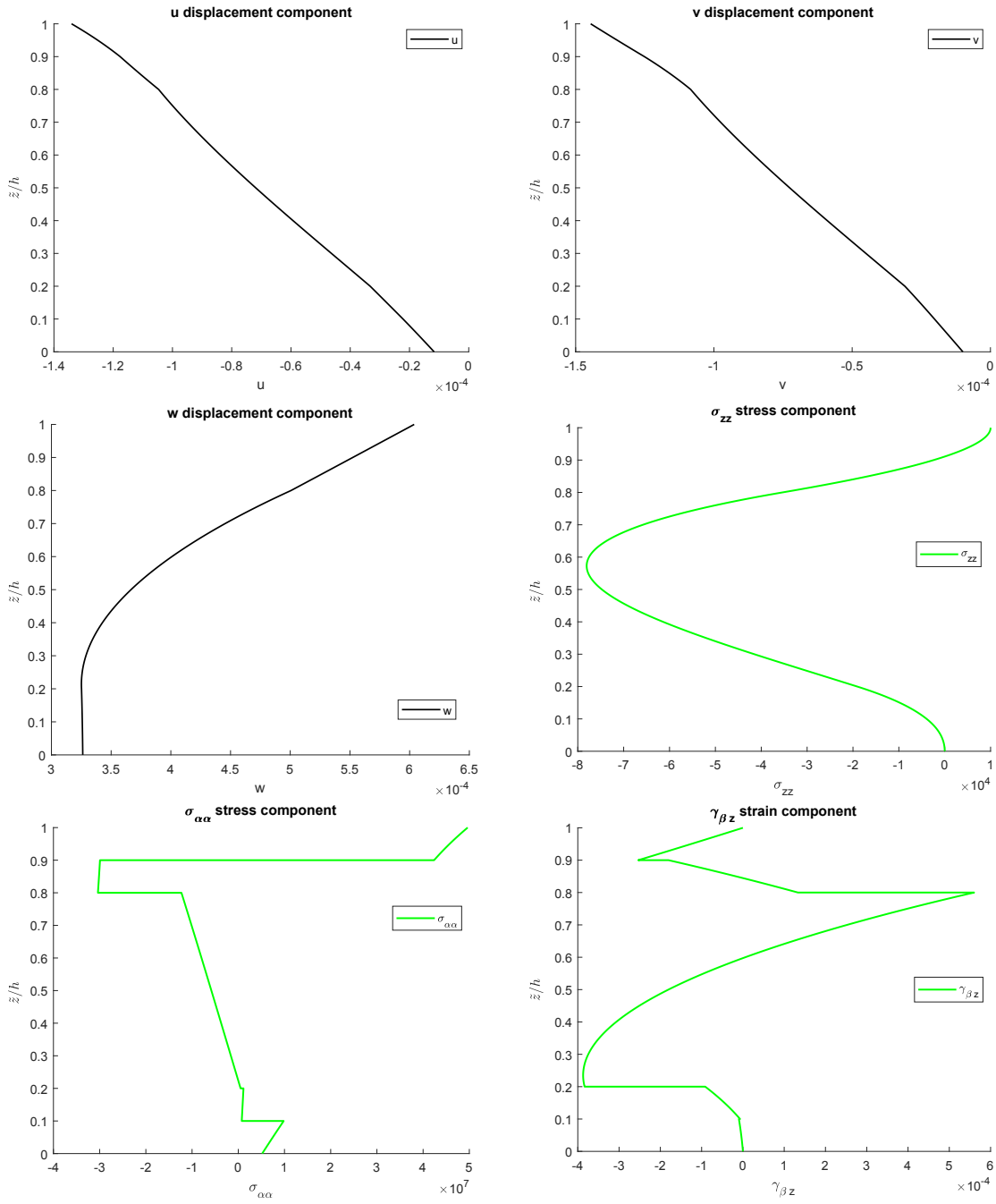

Figure 3: First benchmark, sandwich square plate with imposed external moisture content and applied mechanical load. Displacements, stresses and strains for moderately thick ($a/h = 10$) structure via the 3D($\mathcal{M}_c, 3D$) model. Maximum amplitudes $w[m]$, $\sigma_{\alpha\alpha}[Pa]$ and $\sigma_{zz}[Pa]$ at ($a/2$, $b/2$), $u[m]$ at (0, $b/2$), $v[m]$ and $\gamma_{\beta z}[-]$ at ($a/2$, 0).

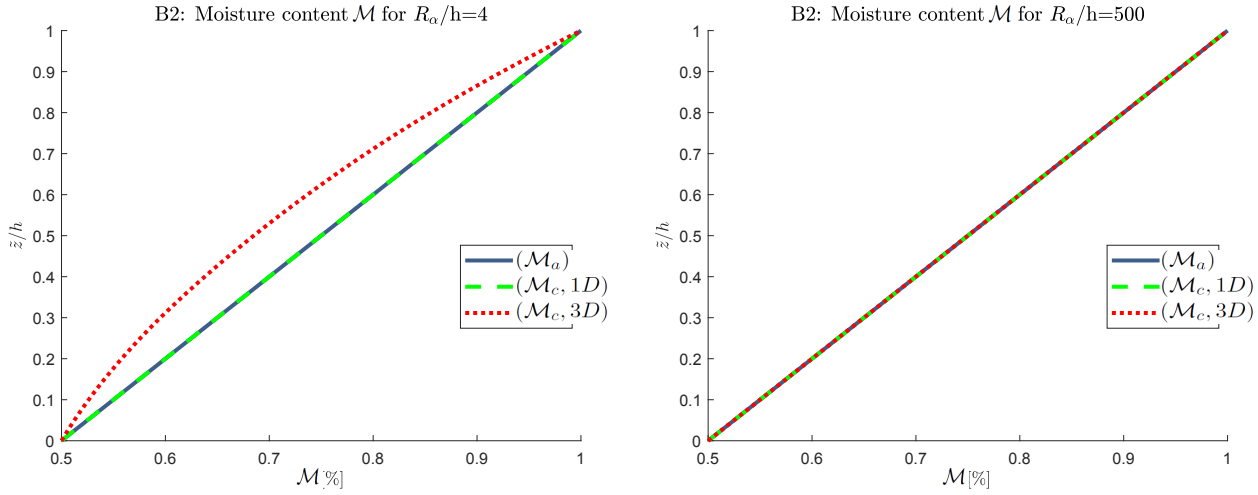

Figure 4: Second benchmark, three-layered composite cylindrical panel with imposed external moisture content: moisture content profiles for thick (on the left) and thin (on the right) structure. The maximum moisture content is evaluated at $(a/2,\, b/2)$.

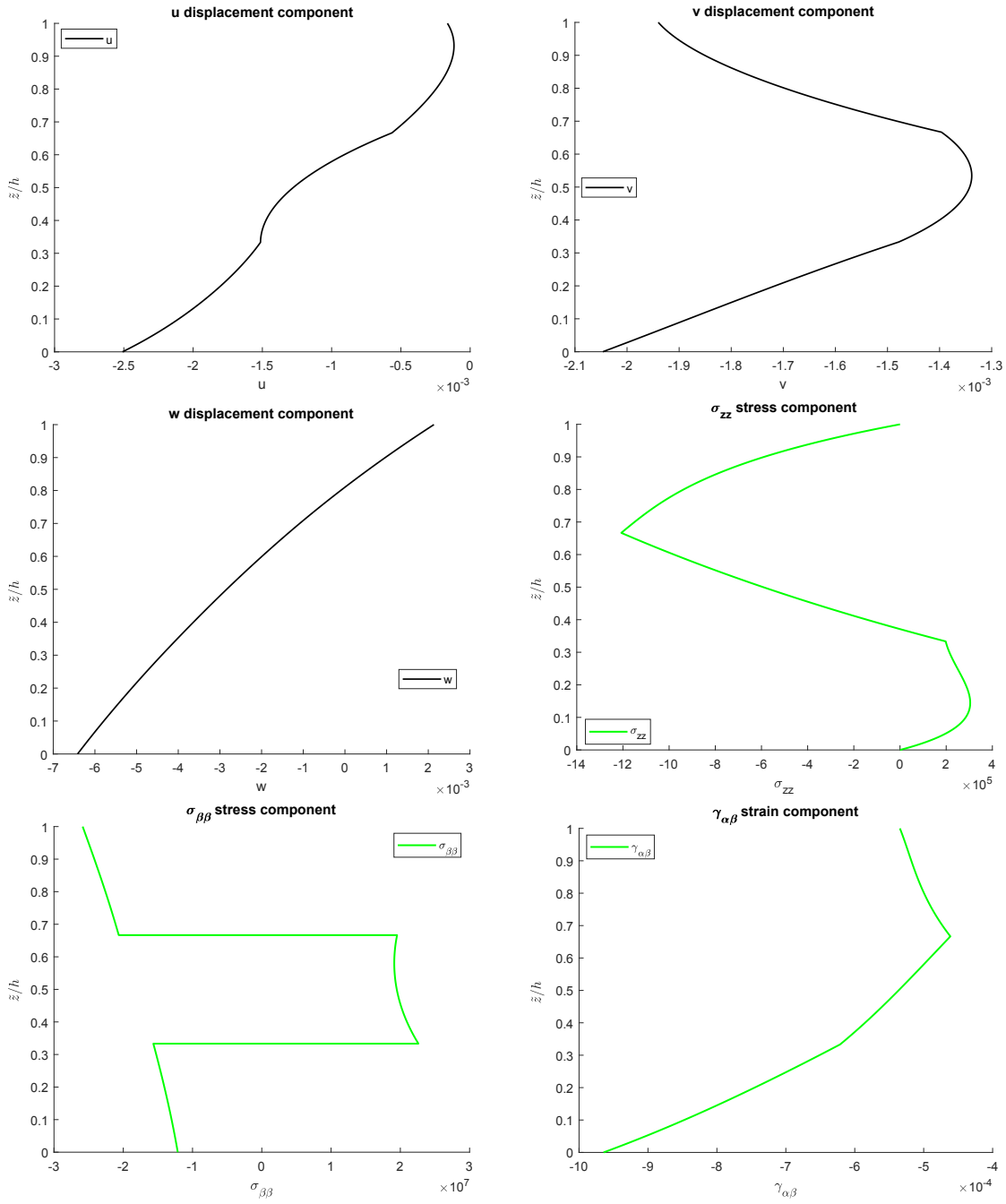

Figure 5: Second benchmark, three-layered composite cylindrical panel with imposed external moisture content. Displacements, stresses and strains for thick structure via the 3D($\mathcal{M}_c, 3D$) model. Maximum amplitudes $w[m]$, $\sigma_{\beta\beta}[Pa]$ and $\sigma_{zz}[Pa]$ at $(a/2,\, b/2)$, $u[m]$ at $(0,\, b/2)$, $v[m]$ at $(a/2,\, 0)$ and $\gamma_{\alpha\beta}[-]$ at $(0,\, 0)$.

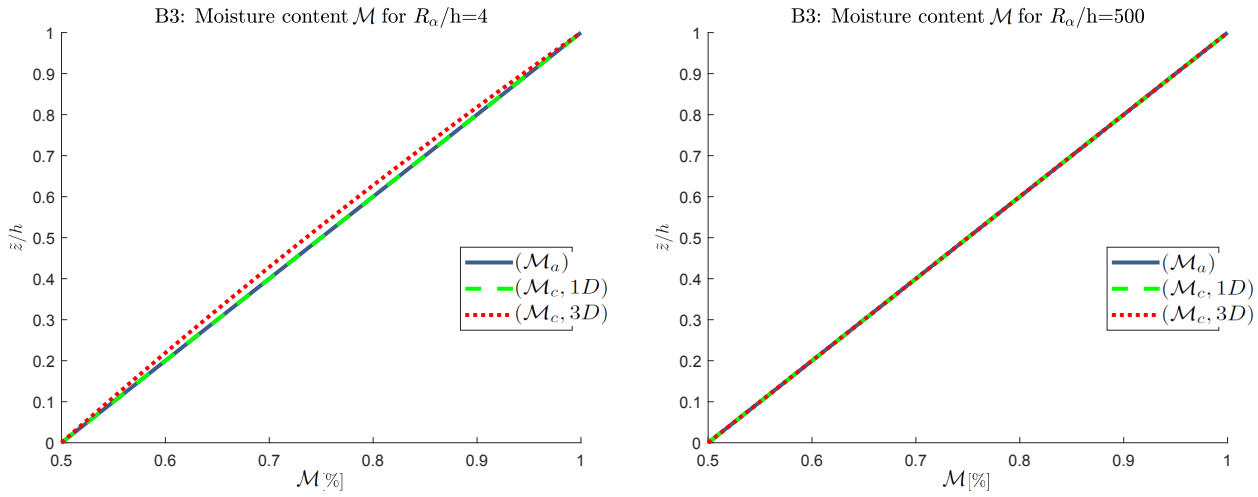

Figure 6: Third benchmark, four-layered composite cylinder with imposed external moisture content: moisture content profiles for thick (on the left) and thin (on the right) structure. The maximum moisture content is evaluated at $(a/2,\, b/2)$.

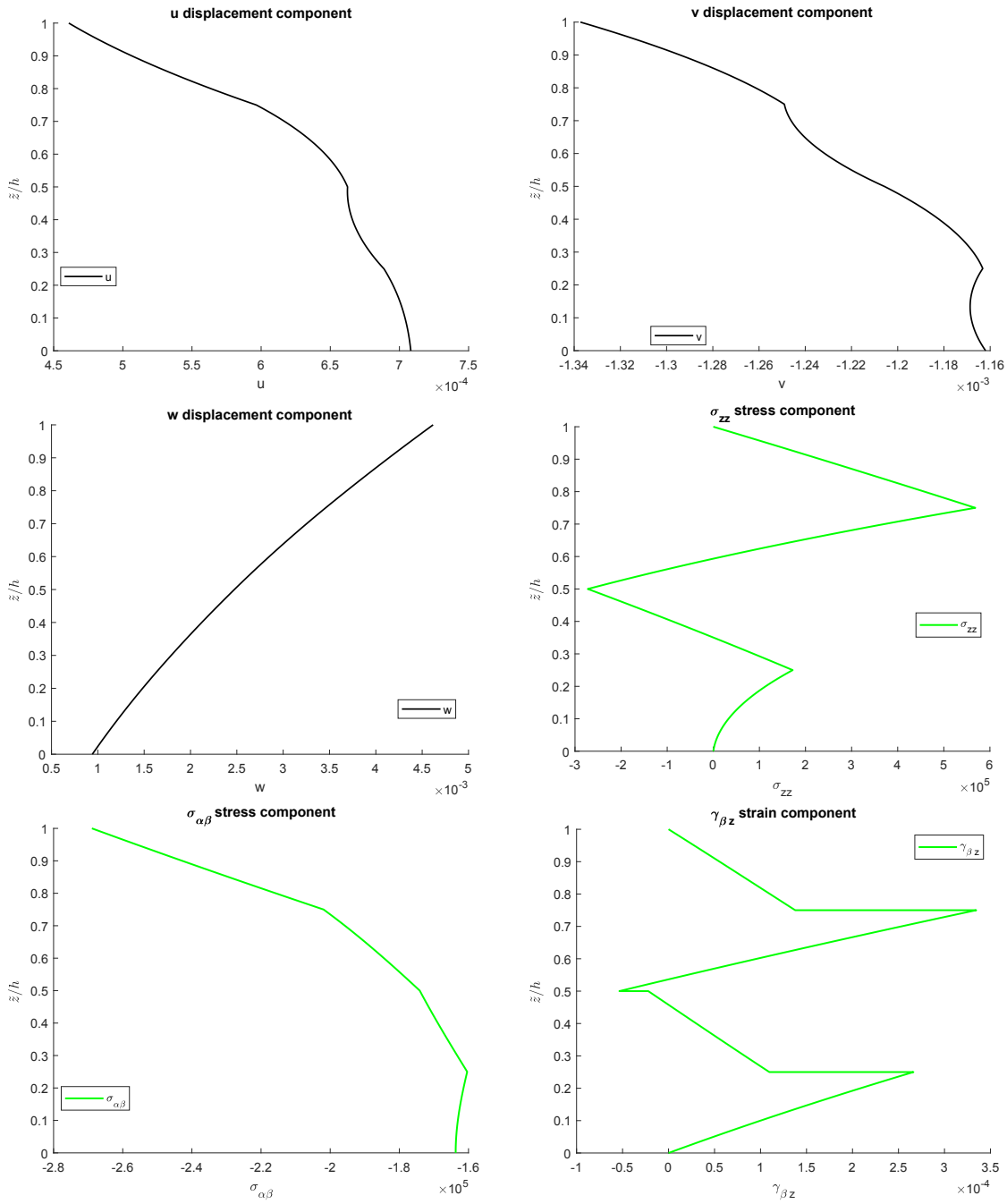

Figure 7: Third benchmark, four-layered composite cylinder with imposed external moisture content. Displacements, stresses and strains for moderately thick structure via the 3D($\mathcal{M}_c, 3D$) model. Maximum amplitudes w[m] and $\sigma_{zz}[Pa]$ at ($a/2$, $b/2$), $u[m]$ at (0, $b/2$), $v[m]$ at ($a/2$, 0), $\sigma_{\alpha\beta}[Pa]$ at (0, 0) and $\gamma_{\beta z}[-]$ at ($a/2$, 0).

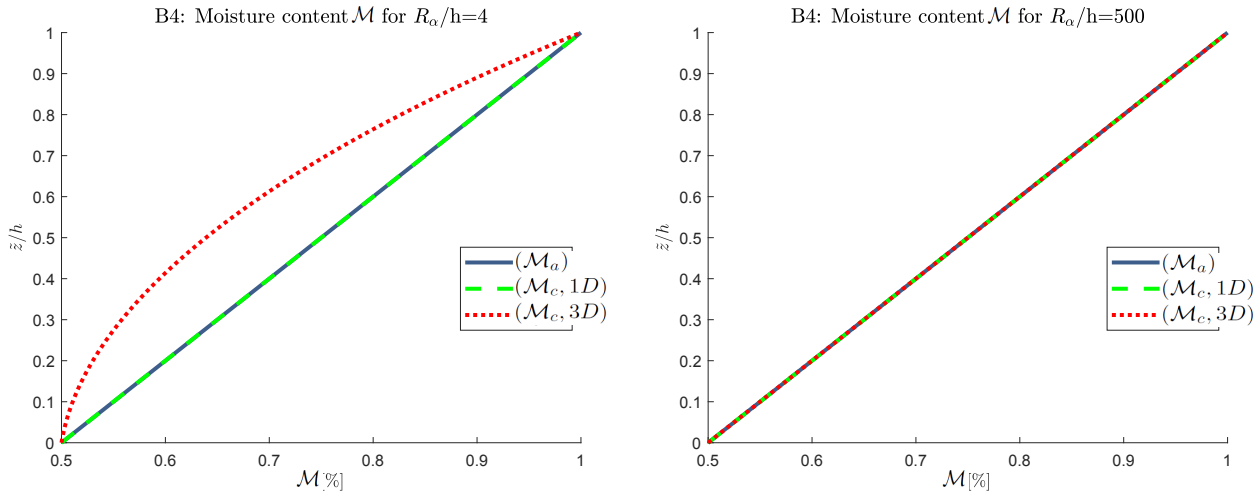

Figure 8: Fourth benchmark, three-layered composite spherical shell panel with imposed external moisture content: moisture content profiles for thick (on the left) and thin (on the right) structure. The maximum moisture content is evaluated at $(a/2, b/2)$.

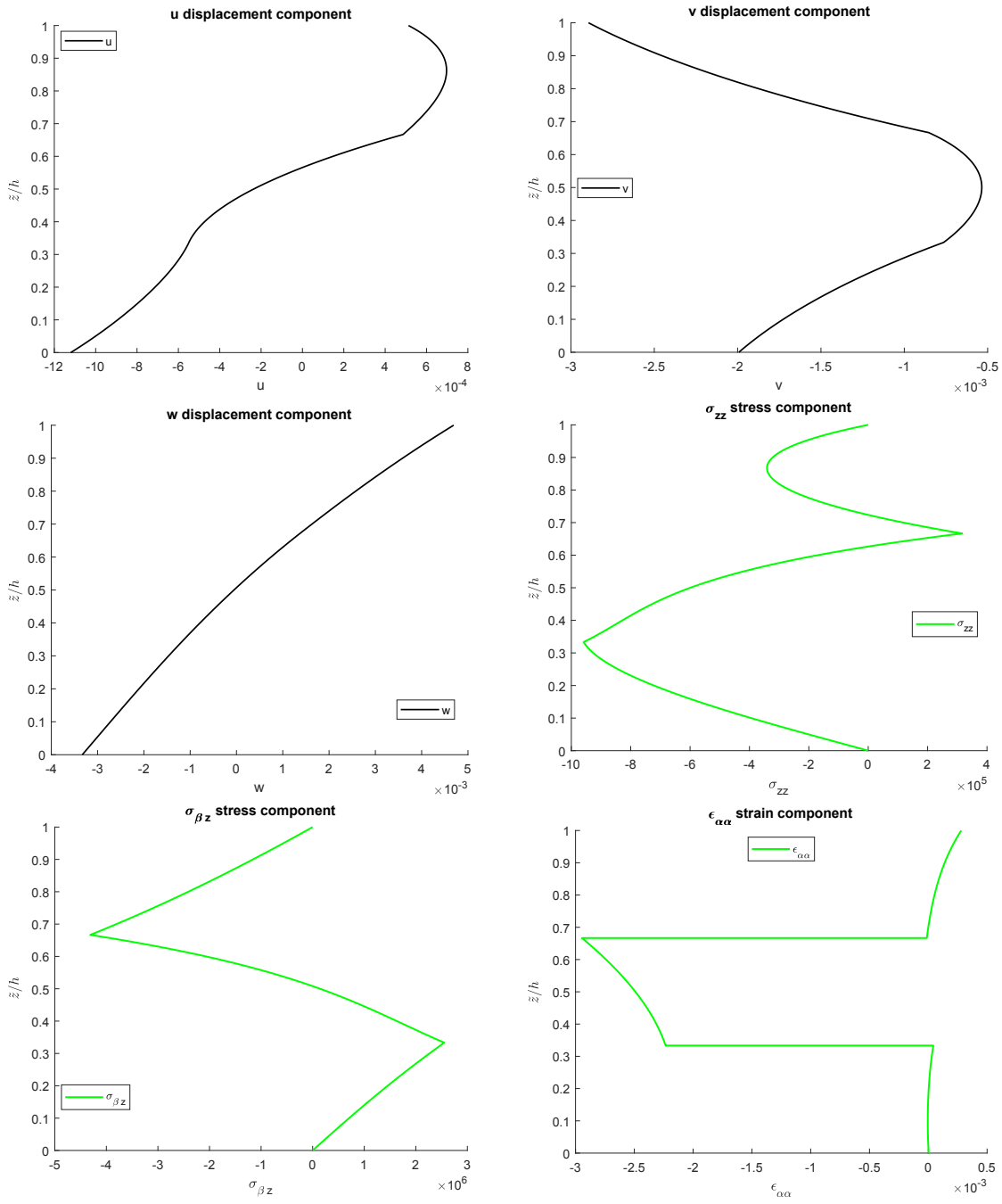

Figure 9: Fourth benchmark, three-layered composite spherical shell panel with imposed external moisture content. Displacements, stresses and strains for thick structure via the 3D($\mathcal{M}_c, 3D$) model. Maximum amplitudes $w[m]$, $\epsilon_{\alpha\alpha}[-]$ and $\sigma_{zz}[Pa]$ at ($a/2$, $b/2$), $u[m]$ at (0, $b/2$), $v[m]$ and $\sigma_{\beta z}[Pa]$ at ($a/2$, 0).